8-25-2016

ASSESSING DROUGHT-INDUCED CHANGE IN A PI\xd1ON-JUNIPER WOODLAND WITH LANDSAT: A MULTIPLE ENDMEMBER SPECTRAL MIXTURE ANALYSIS APPROACH

William Brewer

Will Brewer

Candidate

Geography and Environmental Studies

Department

This thesis is approved, and it is acceptable in quality and form for publication:

Approved by the Thesis Committee:

Caitlin L. Lippitt , Chairperson

Christopher D. Lippitt

Marcy E. Litvak

ASSESSING DROUGHT-INDUCED CHANGE IN A PIÑON-JUNIPER WOODLAND WITH LANDSAT: A MULTIPLE ENDMEMBER SPECTRAL MIXTURE ANALYSIS APPROACH

BY

WILLAM L. BREWER

B.A. Geography, Texas Tech University
2012

THESIS

Submitted in Partial Fulfillment of the
Requirements for the Degree of

Master of Science

Geography

The University of New Mexico
Albuquerque, New Mexico

July, 2016

ACKNOWLEDGMENTS

I heartily acknowledge Dr. Caitlin Lippitt, my advisor and chair, for continuing to encourage me through the months of analysis and writing it took to complete this research. Her guidance and professional style will remain with me as I continue my career.

I also thank my committee members, Dr. Chris Lippitt, and Dr. Marcy Litvak, for their valuable recommendations pertaining to this study and assistance in my professional development.

Gratitude is extended to the people in the Litvak Lab and GEM Lab for the data and analysis help, thank you.

And, finally, thank you to my girlfriend, Marie Westover. Your love and dedication will always be appreciated.

Assessing Drought-Induced Change in a Piñon-Juniper Woodland with Landsat: A Multiple Endmember Spectral Mixture Analysis Approach

By

William L. Brewer

B.A. Geography, Texas Tech University, 2012

M.S. Geography, University of New Mexico, 2016

Abstract

Piñon-juniper communities exist on mid-elevation mountain ranges throughout the southwestern United States. Drought adapted, these species have lived with climatic stochasticity since the end of the Pleistocene. However, increasing temperatures and drought within the last two decades have stressed this community beyond its adaptive limits. With increased drought-induced stress, piñon show greater vulnerability to die-off than juniper. Widespread piñon die-off occurred during 2002-2004 from extreme drought in northern New Mexico with minimal juniper die-off.

This study quantified the differential piñon and juniper mortality during the 2010-2013 drought at a site in central New Mexico by performing multiple endmember spectral mixture analysis (MESMA) on six Landsat images from 2009 through 2015 using field-based spectral endmembers collected throughout 2015. An ideal spectral seperability date was identified to maximize separation between constituent land cover classes by calculating NDVI, SAVI, and RENDVI for the five dominant land cover classes at the site (juniper, piñon, dead piñon, herbaceous, and bare soil) and analyzing

precipitation and temperature data. Peak seperabililty between land cover classes was determined to occur during the pre-monsoon season between late spring/early summer (May) when no spectral overlap occurred between classes ($\sigma = 1$). The field-based reference endmembers were then used to unmix each image in the study period. Results indicate a 24.6% decline in piñon fractional cover across the study period with a comparable 23.8% increase in dead piñon fractional cover and minimal 5.9% change in juniper fractional cover. Accuracy assessment validation using high spatial resolution (5-8 cm) imagery for 2014 and 2015 showed a high degree of confidence in modeled fractional cover results during 2014 - GV (piñon and juniper together) ($R^2 = 0.632$) and dead piñon ($R^2 = 0.854$), and 2015 - GV ($R^2 = 0.735$) and dead piñon ($R^2 = 0.881$). Results indicate the utility of MESMA to monitor and quantify the differential die-off piñon and juniper at a regional scale as climate change-induced drought and higher temperatures are projected to continue in the Southwest.

Contents

List of figures

List of Tables

Chapter 1

Introduction

1.0 Introduction and Background

Climatic variability is a natural component of the environment in the Southwestern United States. Fluctuations in rainfall and temperature have influenced the evolution of drought tolerant traits for millennia. Drought tolerant species like the piñon pine (*Pinus edulis*) and one-seed juniper (*Juniperus monosperma*) have thrived. Occupying a range of 100 million acres across the West (Romme et al. 2009), piñon-juniper woodland (hereinafter referred to as PJ) is one of the most widely distributed cover types in the Southwest and also one of the most heavily impacted by drought. Recent large-scale severe droughts combined with higher temperatures have stressed PJ communities beyond their adaptive limits (Breshears et al., 2005; Breshears et al, 2009; Williams et al, 2013). As temperatures and drought are predicted to increase (IPCC, 2014) in the Southwest United States, monitoring the effect of disturbance events on the spatially extant and ecologically significant PJ communities has critical importance. Analysis of moderate spatial resolution remotely-sensed imagery such as Landsat offer the ability to quantify the scope and rate of change of this critical plant community across the Southwest (Xiao et al., 2005; Yang et al., 2012). This thesis aims to 1) determine what time of year are piñon and juniper most spectrally separable from the surrounding environment, 2) determine how precipitation influences the timing of separability between PJ and the surrounding environment, and between piñon and juniper, 3) determine if piñon pine (*Pinus edulis*) and one-seed juniper (*Juniperus monosperma*) spectrally separable in Landsat imagery using MESMA, and 4) determine if MESMA can

be used to detect a change in the proportion of piñon and juniper between 2009 and 2015 on the Deer Creek Plateau in central New Mexico.

Drought and high temperatures affect plant communities in a variety of ways. Stress on plant hydraulic systems hampers carbon uptake and metabolism, increasing the likelihood of carbon starvation (Zeppel et al., 2012). A prolonged drought can also result in low water potentials, raising the potential for xylem cavitation, leading to plant death (Rennenberg et al., 2006). Trees not directly killed but weakened by drought have increased vulnerability to infestation from pathogens and pests such as pine bark beetles (Allen et al., 2010). A greater number of host trees leads to larger insect/pathogen population outbreaks, which are exacerbated by longer breeding seasons resulting from warmer average annual temperatures (Raffa et al., 2008). Increased surface temperatures combined with more severe droughts are expected to increase the probability of insect outbreaks in western North American forestland (Logan et al., 2003). The correlation between insect outbreaks, physiological stress from higher temperatures, and more frequent drought indicate that climate change is likely to result in increased tree mortality in the Southwest (Williams et al. 2013).

Two of the most widely studied species that have been impacted by drought-induced tree mortality in the Southwest have been the piñon pine (*Pinus edulis*) and one-seed juniper (*Juniperus monosperma*) (Breshears et al., 2005; Clifford et al., 2011;Gaylord et al., 2013). An expansive co-occurring species, PJ form a dominant regional cover type that can be found between 4,500-8,500 feet above mean sea level (AMSL) from southern Wyoming to northern Mexico and from western Oklahoma to Eastern California (Figure 1). The community is dominated by a PJ overstory but contain

a variety of C4 grasses (e.g. *Bouteloua spp.)* and succulents (e.g. *Opuntia* spp.) in the understory. PJ distribution and composition has been heavily influenced by drought which has persisted in the Southwest since the mid-1990s (Shaw et al., 2005). PJ saw significant composition changes across 1.5 million ha of its range from a particularly severe 1999-2002 drought period. Drought impact was disproportionate between piñon and juniper, with piñon experiencing 40-95% mortality while juniper experienced 2-25% mortality (Breshears et al., 2005, Shaw et al., 2005, Williams et al., 2010). The differential mortality rate is further accentuated when larger, more reproductively mature piñon trees are considered. More mature trees (basal trunk diameter (BTD) >12) experienced a 200-600% greater mortality rate than smaller (BTD <12cm) trees (Mueller 2005).

Widespread and disproportionate mortality of both piñon and juniper indicates a fundamental change in the spatial extent of PJ woodland as well as species composition. Stand structure has experienced a significant shift towards juniper and juvenile (non-reproductive) piñon, resulting in lower canopy height and average stem diameter within the system (Clifford et al., 2008). This composition change in the two dominant overstory species impacts a variety of ecological and physical processes present within these systems with widespread changes to soil water content, light infiltration, and soil nutrient content (Clifford et al. 2008, Rich et al. 2008). Monitoring PJ die-off at the regional scale is critical for understanding these underlying systemic transformations within the biome.

The effects of climate-induced disturbance are distributed across a variety of spatial scales, from the local to the regional, and are not equitably distributed. A host of local abiotic factors, including microclimates, topography, and geology affect the scope

and impact of disturbance events. Drought induced mortality of piñon during the 2002-2003 drought showed significant spatial variability. Piñon mortality was 1.2 % in the southern portions of its range (Manzano Mountains) of the Middle Rio Grande Basin (MRGB) in New Mexico, compared with mortality rates as high as 62% in northern sections of the MRGB (Clifford et al., 2008). The cause of the regional variability is unknown.

With the onset of the 2011-2014 drought, spatial variability may again exist in the extent of piñon die-off throughout the MRGB. Drought intensity during this period was severe (Figure 2). The lowest Palmer Drought Severity Index (PDSI) value on record (-7.23) for the Central Highlands of New Mexico (which overlays the eastern portion of the Middle Rio Grande Basin) recorded during 2011 (South Central Climate Science Center, 2013). PDSI is useful at measuring long-term droughts on a scale with 0 as normal, above average moisture conditions as positive numbers and drought depicted as negative numbers; a value of negative 1 is mild drought, negative 2 moderate drought, negative 3 severe drought, and negative 4 is extreme drought (Palmer, 1965). A value of -7.23 represents exceptional drought.

The effects of drought on PJ woodland manifest at different rates with stress not always immediately apparent. Gaylord et al. 2013 recorded piñon death from beetle infestation one year after drought onset. Temporal lags of the effect of drought on PJ stress may exist in other forms as well. Piñon trees weakened from associated drought and temperature increase may succumb to stress even after a drought has ended (Litvak, personal communication).

PJ is an essential component in these semi-arid woodland ecosystems. The communities provide several ecological and cultural benefits to the natural and human environment. They help regulate soil moisture content, act as carbon sinks, and provide habitat for endangered species (e.g. Gray Vireo) as well as endemic plants. Culturally it provides locally sourced food (pine nuts), firewood, and aesthetic beauty to the Southwest. Given the widespread distribution of PJ throughout the Southwest and its sensitivity to drought, developing effective mapping and monitoring techniques at the regional scale becomes critical, especially considering its importance to the ecosystem and regional culture.

1.1 Research Objectives and Questions

With two drought periods in the last 15 years and more drought unequivocally predicted across the Southwest (IPCC, 2014), the need to examine change in the distribution and composition of piñon and juniper is critical to understanding the effects of drought on PJ communities across the Southwest. Research questions are aimed at evaluating the potential of field spectroscopy of dominant vegetation species in PJ communities as inputs for MESMA of Landsat data to monitor change in PJ communities across the Southwest.

1. What time of year are piñon and juniper most spectrally separable from the surrounding environment?
2. How does precipitation influence the timing of separability between PJ and the surrounding environment, and between piñon and juniper?

3. Are piñon pine (*Pinus edulis*) and one-seed juniper (*Juniperus monosperma*) spectrally separable in Landsat imagery using MESMA?
4. Can we use MESMA to detect a change in the proportion of piñon and juniper between 2009 and 2015 on the Deer Creek Plateau in central New Mexico?

1.2 Background

Remote sensing technologies offer wide utility in monitoring PJ distribution across large spatial extents. PJ distribution has been studied extensively with field-based methods, utilizing plot and line-intercept techniques (Padien et al. 1992; Miller et al. 2008). While these techniques provide a detailed inventory of species richness and abundance, they are labor intensive, making them impractical to implement at large scales. Collected at spatially and temporally consistent intervals, satellite-based remote sensing offers physically based methods to monitor PJ distribution in a precise, reproducible manner. Landsat provides the spectral and temporal resolution necessary to perform most image-based analysis techniques at a moderate (30 x 30 m) spatial resolution. Archived remotely sensed imagery allows for comparison of vegetation composition and distribution through time. Previous mortality events can be explored in relation to drought episodes, shedding light on potential temporal patterns of PJ mortality related to drought stress.

1.2.1 Vegetation Phenology

Successful remote sensing hinges upon the ability to differentiate target materials. For remote sensing of vegetation, identifying when natural variation in the environment best maximizes target differentiation is key to improving results (Woolley 1970). Phenology refers to the timing of cyclical biological phases in plants and how they are influenced by seasonal and interannual variation in the climate and physical environment. Some examples of phenological phases (phenophases) in plants include germination, leaf emergence, flowering, and senescence. Environmental factors and seasonal variation greatly influence the timing, duration, and outcome of phenophases.

In water limited Southwestern dryland systems, plants display significant interannual phenophase variation depending on water accessibility (Duncan et al. 1993; Franklin et al. 1993). Understanding seasonal variation in the environment is essential for timing image collection in order to maximize separability between vegetation types. The evergreen piñon and juniper maintain relatively even phenology throughout the year, displaying minimal variation in spectral properties between the wetter summer monsoonal period and drier fall and spring seasons. However, piñon and juniper show different physiological reactions to drought that may help to spectrally differentiate them. The isohydric piñon are more likely to stop photosynthesizing earlier in response to drought stress by closing their stomata than the anisohydric juniper (Plaut et al., 2012; Limousin et al., 2013). Piñon are more likely to take advantage of wetter periods than juniper, however they must close their stomata more quickly in drier periods, indicating a stronger reaction to moisture deficit when compared to juniper (McDowell et al., 2008; Petrie et al. 2016).

In contrast, surrounding forbs and grasses exhibit markedly different phenophases with unique spectral signatures coinciding with annual seasonal changes in precipitation. Photosynthetic activity in grasses and forbs is driven by seasonal summer monsoonal precipitation events with senescence occurring outside the summer monsoon. Identification of vegetation cover types in remotely sensed imagery can be greatly improved with knowledge of specific phenophases considering germination, leaf emergence, flowering, and senescence can vary greatly between cover types (Franklin 2002). Successfully distinguishing PJ from the surrounding environment and P from J requires knowledge of the interaction of regional climate and annual weather variation on species specific phenophases.

1.2.2 Vegetation Mapping

A variety of remote sensing methodologies have been applied to measure the distribution of vegetation in arid environments. Vegetation indices have been developed to take advantage of the unique reflectance signature of plants in the NIR and visible. Researchers have typically assumed that the chlorophyll content of leaves are proportional to moisture content (e.g. Tucker, 1977; Paltridge & Barber, 1988; Illera et al., 1996).One of the most popular, the normalized difference vegetation index (NDVI) (Eq. 1), is commonly used to estimate the amount of photosynthetic activity by simply taking the difference of the red and NIR band then dividing it by its sum (Tucker, 1979).

$$\mathrm{NDVI} = \frac{(NIR-RED)}{(NIR+RED)} \quad (1)$$

However such indices commonly overestimate photosynthetically active vegetation in semi-arid environments (Kremer et al., 1993; Peters et al., 1995). NDVI was shown to be less effective at retrieving estimates of tree cover and monitoring change in recently disturbed PJ woodland (Yang et al., 2012). In semi-arid systems, sparse vegetation can increase the proportion of soil background reflectance which confounds the index, rendering it less effective at measuring photosynthetically active vegetation (Eitel et al., 2009).

1.2.3 Mixed Pixels

Mixed pixels are an endemic problem in remotely sensed imagery. H – resolution scenes are composed of features larger than the spatial resolution and can, therefore, be resolved (Cracknell, 1998). Whereas, L – resolution scenes are composed of features smaller than the spatial resolution and, thus, cannot be resolved. When the scene resolution is larger than the materials that compose it, the ground elements in that pixel are "mixed", meaning they are composed of more than one material (Strahler et al. 1986). At all resolutions, mixed pixels can misrepresent spatially explicit landcover. However, analysis techniques have been developed to determine the subpixel landcover content for moderate spatial resolution image data: Spectral Mixture Analysis (SMA) and its more powerful extension, Multiple Endmember Spectral Mixture Analysis (MESMA).

1.2.3.1 Spectral Mixture Analysis

SMA is a physically based approach using the spectral signature of a pixel to determine its component parts by predicting the proportion of a pixel that belongs to a class based on the spectral signatures of endmembers (Adams, et al., 1995; Roberts, et al., 1998a). It estimates the proportion of spectral endmembers that could produce the reflectance observed for a pixel. Endmembers are "pure" spectra that correspond to a landcover class. Endmembers can either be collected from the image (image endmembers) or from in situ field measurements (reference endmembers). These endmembers are typically composed of green vegetation (GV), non-photosynthetic vegetation (NPV), soil, and shade components for a natural system (Adams et al., 1993). The number of endmembers SMA can model is limited by the dimensionality of the image to N+1, where N is the number of spectral bands (eq. 2) (Adams et al., 1993). SMA can be expressed as:

$$R_i = \sum_{k=1}^{n} f_k \, R_{jk} + \varepsilon_i \qquad (2)$$

where i is the number of spectral bands used; $k=1, \ldots,$ n (number of endmembers); R_i is the spectral reflectance of band i of a pixel, which contains one or more endmembers; f_k is the proportion of endmember k within the pixel; R_{jk} is the spectral reflectance of endmember k within the pixel on band i, and ε_i is the error for band i. Heterogeneous environments are challenging to unmix at a species level using SMA. Evergreen dominated PJ systems offer phenological phases in which it may be possible to model piñon and juniper as GV, and understory herbs and grasses and dead piñon as NPV. Shade fractions can help distinguish overstory vegetation from understory vegetation (Roberts et al., 2002). However, SMA is limited by its use of one set of

endmembers to model all pixels. This limitation inhibits the model from unmixing spectrally diverse environments like semi-arid woodlands. In response, Multiple Endmember Spectral Mixture Analysis (MESMA) has been developed to allow the number and type of endmember to vary per pixel across an image (Roberts et al. 1998).

1.2.3.2 Multiple Endmember Spectral Mixture Analysis

MESMA functions similarly to SMA except that it accounts for within endmember variability by allowing for multiple definitions of each endmember class (Roberts et al., 1998). By allowing for increased spectral endmember variability, MESMA overcomes the SMA limitation of using the same endmembers to model all pixels whether the endmember is present in the pixel or not (Roberts et al., 1998; Myint & Okin 2009). MESMA models all possible combinations of soil, GV, and NPV endmembers and allows for a variable number of endmembers to solve a given pixel. Optimum models are selected based on best spectral fit and overall best fractional and residual constraints set by the user. MESMA has successfully been applied to map plant species distribution in semiarid environments (Roberts et al., 1998; Okin et al.2001; Dennison & Roberts, 2003; Quintano et al. 2013). MESMA utilizes a spectral library made of image or reference endmembers. Reference endmembers, obtained directly from the environment, offer an advantage over image derived endmembers; they offer absolute modeled fraction estimations because they are a purer in-situ representation of a material, (Drake et al., 1999). The library can be composed of a large number of samples from any cover type to represent soil, GV, and NPV.

Chapter 2

Methodology

2.0 Overview

Field spectra were collected at a PJ site in Central New Mexico throughout 2015 to provide temporal and spectral data for discriminating between target land cover classes. Spectral libraries were generated from field spectra for input to MESMA applied to Landsat data. MESMA was used to model vegetation life form distribution and composition within at the site annually from 2009 to 2015. Change in vegetation cover proportions was quantified and evaluated with respect to drought conditions over the study period. Accuracy of modeled results was assessed against high spatial resolution airborne imagery acquired in 2014 and 2015.

2.1 Study Area

This research site was at the Deer Creek Plateau, hereafter referred to as DCP, located south of the city of Mountainair, New Mexico at approximately 34 26’18.420” N, 106 14’15.698”W (Figure 3). The elevation at the top of the plateau averages 2190 m. The soil across the plateau is Turkey Springs stony loam, primarily characterized by alluvially deposited limestone (Soil Survey Staff). The regional climate is semi-arid, with a mean annual precipitation of 372mm (+/- 86.8 mm standard deviation, sd) and mean, max, and min temperatures of 19.8C (+/- 0.77C sd) and 2.32C (+/- 0.64C sd)

respectively, over the past 20 years (PRISM Climate Group, Oregon State University, http://prism.oregonstate.edu, created 28 June 2004). The site primarily receives moisture from winter snow melt (January to March) and summer monsoon (late July through September). Precipitation varies substantially from year to year, influencing soil moisture levels and the onset of phenophases.

Vegetation across the plateau is semi-arid woodland dominated with a piñon pine (*Pinus edulis*) and one-seed juniper (*Juniperus monosperma*) overstory and an understory characterized by perennial C4 grasses and annual forbs. The DCP is the site of a long-term biological field station (Dr. Marcy Litvak, UNM Department of Biology) situated amongst a low density housing development. Research on the site has focused on long-term PJ manipulation studies that provide an ideal assortment of in situ data to corroborate remote sensing analyses.

2.2 Data

2.2.1 Landsat Imagery

The principal analysis imagery used in this study was acquired from the Landsat Ecosystem Disturbance Adaptive Processing System (LEDAPS) (http://earthexplorer.usgs.gov/). All Landsat scenes were processed to level L1T and atmospherically corrected using an absolute correction method (MODTRAN). Image values were recorded in surface reflectance (0-10,000). One cloud-free scene was selected from path 33, row 36 for each year that fell within two weeks of the ideal separability date (May 7th) and at least one week from major precipitation events (Table

1). Imagery from 2009-2011 was collected with Landsat 5 TM while 2013-2015 imagery was collected from Landsat 8 OLI. Image data from 2012 was omitted due to the unavailability of complete data from the Landsat 7 scan line corrector failure.

2.2.2 Field Spectroscopy

Reference endmembers were collected from field-based reflectance measurements using a field spectrometer (ASD Fieldspec 4® Standard Resolution Spectroradiometer). The spectrometer has a spectral range of 350-2500 nm. It collects in the visible and near-infrared (350-1000 nm) at a 3 nm full width half maximum and the short wave infrared (1000-2500 nm) at a 10 nm full width half maximum. Five cover types were identified as primary scene constituents: piñon (P), dead piñon (DP), juniper (J), herbaceous (H), and bare ground (soil). Collections were made at five dates throughout 2015 to determine the optimal date to maximize cover type separability.

Sites representative of each cover type were selected within close proximity to the PJC (Figure 4). Site selection was based on unobstructed solar illumination +/- 2 hours of solar noon (10 am- 2 pm) and on minimal interference from background scattering of surrounding vegetation. Sites were spread out to capture local topographic variability accessible within a limited 4-hour collection window (Figure 4). Real Time Kinematic (RTK) GPS coordinates were recorded for each location to ensure their location was known for future measurements. All selected P and J sites were mature trees with no chlorosis or partial mortality present. DP sites were mature standing-dead trees composed of completely defoliated non-photosynthetic woody material. H sites were

selected based on complete, homogenous ground cover of the same grass species type (e.g. *Bouteloua spp.)* which were then aggragated together to form the H class. Bareground (soil) sites were selected for open bare soil away from tree coverage or water drainages. A higher proportion of P (n=20), DP (n=20), and J (n=10) sites were selected to capture greater signature variability. Fewer soil (n=2) sites were selected due to pseudo-invariability across the plateau and high spectral separability between soil and the vegetation classes. Similarly, fewer H (n=5) sites were selected due to high interclass spectral separability (Table 2).

Five spectra collections were made throughout 2015. Each date was spaced approximately two months apart to capture seasonal phenological changes across the site. All collections were made under cloud free conditions. The spectrometer was standardized to a Halon white reference panel every 10 minutes or with a change in collection location. Reflectance measurements were collected 20-30 cm above each target with the sensor positioned at nadir. Measurements were recorded using a 25° field-of-view optic, creating an 8-16 cm diameter footprint. Spectra were collected at each site based on homogeneity of cover within the field-of-view optic (i.e. densely leafed branch, dense grass cover, etc.). Seasonal changes in illumination and daily fluctuations in shadow could change the location of spectra collection at each site. However, care was taken to ensure that spectra collection locations (i.e. individual branches) were representative of the site as a whole. Spectra collections were taken at the same sites throughout the study period. Ten reflectance recordings were made for each target at two second intervals. The May 7th collection contained fewer spectra recordings (10 samples/site, instead of 30) due to a battery failure during that collection date.

2.2.3 Accuracy Assessment

2014 and 2015 MESMA results were assessed for accuracy using true color high spatial resolution (5-9 cm) imagery collected over the Deer Creek Plateau September 2-4, 2014 and October 13-15, 2015 using a 2x Canon 5D Mark II fixed to a light wing aircraft. Both imagery dates were geometrically corrected and show a high coregistration level (<1 m error) by the GIScience for Environmental Management (GEM) Lab at the University of New Mexico.

2.3 Preprocessing

2.3.1 Landsat Preprocessing

All Landsat scenes were georeferenced prior to download to a L1T Level 1 Product Generation System (LGPS) standard which includes terrain corrected processing of approximately 128 GCPs w/ <0.5 RMSE. Six band (blue, green, red, NIR, SWIR1, and SWIR2) image stacks were generated for each date. The imagery was then subset to the extent of the DCP study area (13.9 km^2).

2.3.2 Field Spectra Preprocessing

Field spectra were evaluated for quality at each collection date using ViewSpec Pro software (*ViewSpec Pro™ User Manual*, 2008). Individual spectra samples displaying dramatic in-class irregularities were removed. The remainder were averaged

by land cover type (i.e. P, J, DP, H, and soil) and by target (1 target = 10 spectra) in ViewSpec Pro. Spectra were then resampled to Landsat bands in ENVI 5.2 image processing software (http://www.exelisvis.com/). All spectra were averaged by land cover class from the May 7th collection date and then convolved to both Landsat 5 TM (bands - 1, 2, 3, 4, 5, and 7) and Landsat 8 OLI (bands – 2, 3, 4, 5, 6, 7).

2.4 Spectral Separability Analysis

The optimal date for distinguishing land cover types was determined through a qualitative separability analysis of vegetation indices and bands. NDVI (eq. 1), SAVI (eq. 3), and RENDVI (eq. 4) were calculated from the averaged class values at all five collection dates. Landsat 5 convolved green, red, and NIR bands were plotted for each class. Sample standard deviations (eq. 5) were calculated from the convolved target averages for each land cover type.

$$SAVI = \frac{(\mathrm{NIR}-\mathrm{RED})}{(\mathrm{NIR}+\mathrm{RED})} * (1 + L) \quad (3)$$

where NIR is the reflectance value of the near-infrared band and RED is the reflectance value of the red band convolved to the corresponding Landsat 5 bands and L is the soil brightness correction factor.

$$\mathrm{RENDVI} = \frac{\rho 750 - \rho 705}{\rho 750 + \rho 705} \quad (4)$$

where $\rho 750$ and $\rho 705$ are the reflectance values at 750 nm and 705 nm, respectively.

$$S = \sqrt{\frac{\sum(x-\bar{x})^2}{n-1}} \quad (5)$$

where S is the square root of the sum of the sample mean ($\bar{x}$) squared, divided by the number of samples (n).

Visual inspection of spectral shape and overlap between classes across the entirety of the spectrum allowed for the assessment of class separability at each collection date. Sample standard deviation error bars (s = 1) were calculated to show the range of data within the mean and provided additional context for determining separability. Spectral libraries were then created in ENVI from all raw spectra from the optimal spectral separability date (May 7th). The library was then convolved to Landsat 5 TM (bands - 1, 2, 3, 4, 5, and 7) and Landsat 8 OLI (bands – 2, 3, 4, 5, 6, 7).

2.4.1 Climate Data

Climate data includes precipitation data sourced from daily collections made at the PJ Control site 2009-2015 (Litvak Lab, University of New Mexico, 2016).

2.4.2 Precipitation and Spectral Separability

Precipitation data was plotted to weekly increments for 2009-2015. Plots were then used to determine: 1) how precipitation (duration, time since last substantial precipitation event, and annual amount) is related to separability between classes and 2) precipitation induced variation in Landsat image dates. Ideal dates of separability

between land cover classes were identified for 2015 by comparing vegetation indices with spectral curves with precipitation data (one week, one month, and time since last precipitation) for the five collection dates. The collection date that occurred during a month with minimal total precipitation and farthest from major precipitation events (>10 mm) was chosen for analysis.

2.5 MESMA

The May 7th field-based spectral libraries were then used as inputs for image unmixing. Multiple Endmember Spectral Mixture Analysis (MESMA) was applied to six Landsat image dates (Table 1) to estimate fractional cover of green vegetation, non-photosynthetic vegetation, and bare ground within the study area.

2.5.1 Endmember Selection

The TM and OLI convolved spectral libraries from the May 7th spectra collection were input to the Visualization and Image Processing for Environmental Research (VIPER) Tools 2.0, an open source extension to ENVI 4.7 used for endmember refinement and MESMA processing (http://www.vipertools.org). Three endmember classes were created to represent the five input land cover types: green vegetation (GV) containing photosynthetic P and J spectra, non-photosynthetic vegetation (NPV) containing H and DP spectra, and soil containing bare ground spectra.

A total of 55 potential endmembers were input into the model before erroneous spectra were removed (29 GV (P=18, J=11), 24 NPV (H=5, 19=DP), and 2 soil).

Potential endmembers input to MESMA are refined by a set of three indexes provided in VIPER Tools: Count based Endmember selection (CoB), Minimum Average Spectral Angle (MASA), and Endmember Average RMSE (EAR) (Figure 5). MASA identifies which spectra best models each class by determining which has the lowest average spectral angle between all other spectra within the same class (Dennison et al., 2004). EAR determines which spectra produce the lowest average RMSE when used to model all other spectra of the same class (Dennison & Roberts, 2003). CoB selects optimal endmembers that best model the other within class spectra (Roberts et al., 2003). Optimal CoB models unmix other spectra in the library within user defined fraction, RMSE, and residual constraints. The total number of spectra modeled within the class (in_Cob) and the total outside the (out_CoB) are recorded for each model. Spectra with the highest in_CoB and lowest out_CoB, EAR, and MASA will be selected for MESMA (Roberts et al., 2003).

EAR can be described in Eq. 6 where *i* is an endmember, *j* is the modeled spectrum, N is the number of endmembers, and n is the number of modeled spectra.

$$EAR_i = \frac{\sum_{j=1}^{N} RMSE_{i,j}}{\mathrm{n}-1} \quad (6)$$

MASA functions similarly to EAR, but uses the spectral angle (θ) for the error metric. The optimum spectra has the lowest average RMSE. MASA can be defined as (Eq. 7):

$$MASA_i = \frac{\sum_{j=1}^{N} \theta_{ij}}{\mathrm{n}-1} \quad (7)$$

In MASA, the spectral angle is defined as the reflectance of an endmember (ρλ), the reflectance of a modeled spectrum (ρ'λ), the length of the endmember vector (Lρ) and the length of the modeled spectrum vector (Lρ'). Length is the square root of the sum of reflectance in each wavelength of the model. The spectral angle is defined as (Eq. 8):

$$\theta = cos^{-1}\left(\frac{\sum_{\lambda=1}^{M} \rho_\lambda \rho'_\lambda}{L_\rho L_{\rho'}}\right) \quad (8)$$

A total of 19 endmember signatures were extracted as the input spectral libraries for MESMA (Figure 6). A total of eight endmembers were selected to represent GV (P=5, J=3), nine endmembers were used to represent NPV (DP=7, H=2), and two endmembers were used for Bare Ground. A shade endmember was not used, but treated as a remainder in the unmixing process. It is assumed to be a unique component of each class with differences image to image.

2.5.2 Application of MESMA

Each Landsat image date was modeled (i.e. unmixed) using MESMA routines in Viper Tools. This unmixing approach estimates the proportions of GV, NPV, and soil per pixel in an image with endmembers from the input spectral library. Output fractional cover images and proportions were used to derive quantitative estimates and maps of vegetation cover.

One-, two-, and three- endmember models were applied to each Landsat image. Two constraints were set for each model, fraction values had to range between -0.05 and 1.05 with a RMSE threshold of 0.025 (Viper Tools User Manual). A pixel was left unmodeled if the constraints were not met. All possible combinations of endmembers

were run for each one-, two-, and three-endmember models (269 total). The optimal model was then selected for each pixel. Optimization was achieved by selecting the model with the fewest endmembers and the lowest RMSE (eq. 9).

$$RMSE = (\sum_{k=1}^{N}(e_k)^2/N)^{1/2} \quad (9)$$

Where N is the number of bands, e_k is the residual term at band k (k= 1,2,….N). In addition to helping fit the model and create endmembers, RMSE can be used as an accuracy assessment tool.

Seven bands of information were generated for each unmixed image. A band containing the fractional cover for each endmember: GV, NPV, soil, and shade as well as bands containing model complexity (one-, two-, or three-endmember), RMSE, and model number (unique ID of endmember combination selected to model each pixel). Following the three endmember analysis of GV, NPV, and soil, another MESMA model was run for P, J, DP, H, and soil as five separate endmembers.

2.5.3 Estimation of Fractional Cover

Total fractional cover was generated by summing each endmember fraction and dividing by the total number of pixels in the study area for each image date. Fractional cover was estimated for three sites: the entire DCP, the PJC (4 ha), and PJG sites (4 ha). Fractional cover for each endmember was summed for all pixels that fell completely within each site to account for co-registration differences between Landsat pixels and site boundaries. Individual bands containing endmember fractional cover estimates for GV, NPV, and soil were output for each study area and date to spreadsheets for quantitative analysis.

2.5.4 Evaluation of Vegetation Change

Percentage of vegetation change was determined for all three sites (DCP, PJC, and PJG) by evaluating fractional cover proportion at each date. Change in proportion of vegetation was calculated between each year and across the study period.

2.6 Accuracy Assessment

The accuracy of MESMA modeled fractions were assessed for 2014 and 2015 using high spatial resolution imagery. Ten 90 x 90 m reference plots were created to a match a 3 x 3 Landsat pixel equivalent to avoid co-registration errors (Figure 7). Plots were randomly distributed across the study site using a simple random pattern distribution model in ArcMap. The simple random distribution pattern reduces user bias and helps ensure topographic and vegetation variability at the site is randomly included in the validation. Validation data of fractional cover was generated using a point-grid sampling method. A dot matrix grid was generated and overlaid on the reference imagery. 441 sample points were laid out per plot (49 points/pixel). Four cover types were discernable in the reference imagery and recorded: piñon/juniper, dead piñon, herbaceous, and soil. Cover types directly coincident to each point were visually determined, recorded, and exported for further analysis.

Three statistical measures (RMSE MAE, and R^2) were used to determine the error between MESMA modeled fractions and cover fractions evaluated in reference plots.

Mean Absolute Error (MAE) provides an average of the absolute errors $|e_i| = |f_i - y_i|$, where f_i is the prediction and y_i the true value, and is provided in the formula (Eq. 10):

$$MAE = \frac{1}{n}\sum_{i-1}^{n}|f_i - y_i| = \frac{1}{n}\sum_{i=1}^{n}|e_i| \quad (10)$$

R^2 regression analysis was used to evaluate how well the MESMA modeled fractions compared to reference data, where SS_{res} is the sum of the squared error and SS_{tot} is the sum of the squared total (Eq.11):

$$R^2 = 1 - \frac{SS_{res}}{SS_{tot}} \quad (11)$$

RMSE, MAE, and R^2 were computed for each plot and averaged. Each endmember was assessed individually. Of the cover types discernable on the assessment imagery, piñon/juniper were grouped as GV, dead piñon/herbaceous were grouped as NPV, and soil as soil.

2.6.1 Evaluating MESMA Differentiation Between Piñon and Juniper

The effectiveness of MESMA at differentiating P and J was determined by comparing MESMA modeled fractions with data from a DCP manipulation study. In September 2009, 1632 adult piñon (>7 cm diameter at breast height) were girdled in a 4 ha plot (girdled site). Juniper at the girdled site were left unaltered. A 4 ha control plot 3 km away was untreated. By the spring of 2010 all adult piñon at the girdled site had died and defoliated. Increased drought mortality and pine bark beetle outbreak killed the other standing immature piñon in the years immediately following the treatment at the girdled

site, leaving the site nearly void of piñon. The control site experienced mortality at a rate similar to the rest of the plateau.

The girdled site provides a site for comparison of MESMA modeled fractions with ground based data. Output models for 2009 for the girdled site should not differ significantly from the control plot in P endmember selection. In the years following 2010 (after complete mortality of girdled piñon) no P endmembers should be selected for modeling pixels inside the girdled site. Modeled fractions at the control site should not differ from those of the surrounding environment. Evaluating the ability of the modeled fractions to reflect the P mortality at the girdled site after 2009 provides a basis for how effectively MESMA can differentiate P from J.

Chapter 3

Results

3.1 Piñon and Juniper Spectral Separability

Mean spectral curves of all spectra collected for each class (P, J, DP, H, and soil) were plotted for each collection date (Figure 8). Separability was visually determined using spectral plots as well as reflectance and vegetation index values (Figure 9). Field-based spectral measurements indicate spectral separability between vegetation types is substantially affected by precipitation events associated with the seasonal summer monsoon, apparent in the substantial increase in precipitation at each year in the study period (Figure 10). The precipitation increase triggers the green up of normally senescent low lying herbaceous vegetation and grasses (primarily C4) while evergreen piñon and juniper do not respond noticeably to seasonal changes in moisture, maintaining relatively consistent spectral signatures throughout the year (Figure 11).

Juniper showed the least amount of change in SVI values throughout the study period. NDVI fluctuated less than 5% between the lowest and highest collection dates (mean NDVI = 0.719 and 0.751, respectively). The P class showed noticeably more variation with NDVI fluctuating 22.6% throughout the study period between the lowest and highest years (mean NDVI = 0.583 and 0.754, respectively). The highest photosynthetic rates for both piñon and juniper occurred during the September and November collection dates (Figure 9).

Peak separability of all spectra occurred during the May collection date for 2015. At this period in the growing season, a high degree of separability was exhibited between bands and vegetation indices for all classes, with particularly high separability displayed between piñon and juniper. No overlap in spectral reflectance occurred between piñon and juniper during the May collection within one standard deviation (Figure 9). SVI values demonstrate that the greatest between class separability occurred immediately before the onset of the monsoon, in May and slightly less so in July. May was also the best date for discriminating piñon and J from other land cover classes as there is also no overlap in reflectance between piñon and J and the other classes using NDVI, SAVI, and RENDVI.

3.2 Evaluation of Precipitation and Spectral Separability

Class separability varied little between soil and the NPV classes (H and DP) throughout all five collection dates with both showing high separability in the Red, Green, and NIR bands of Landsat. Similarly, soil showed minimal overlap with the GV classes, (P and J).

At the February recording date, the H class displayed the highest reflectance values in the green and red bands (0.11 and 0.14, respectively) (Figure 9) across all five collection dates, indicating a low concentration of photosynthetic pigments. The November collection had the second highest reflectance in the red and green bands (0.13 and 0.16, respectively). The lowest spectral vegetation indices (NDVI, SAVI, and RENDVI) were recorded during the February collection and second lowest during the

November collection, representing low photosynthetic activity during months farthest from the monsoon.

Collections made during May, July, and September showed noticeably greater photosynthetic activity in the spectral reflectance curves of the H class (Figure 9). The highest SVI values occurred during July, coinciding with the early monsoon period. The highest SVI values for the H class were recorded at the July collection. Following peak photosynthetic activity, the H class bands and SVIs (σ=1) displayed some overlap with the soil and DP classes during the period of little to no photosynthetic activity (fall and early winter).

Warmer spring temperatures and modest precipitation provided enough moisture for sufficient photosynthetic activity in the H class, allowing for spectral separation from the soil and DP classes without confusion with the P and J classes (Figure 11). Prior to the May 7th spectra collection, 15 mm of rain fell within the previous week and 26.5 mm within the previous 31 days. Only five days separated the collection date from the closest previous measureable (>1 mm) rainfall event.

The spectral response of P and J display less variation than the H class throughout the study period. However, little precipitation during late winter and early spring reduced the photosynthetic activity of the P class during May, allowing for spectral separation from the J class. A total of 76.5 mm of precipitation fell from January to May, compared to 243.58 mm from July through November. During the 31 days immediately prior to the May collection, only 26.5 mm of precipitation fell. That amount is similar to the 18.6 mm recorded during the 31 days prior to the February collection which saw similarly low SVI values for the P class. In contrast, September and November saw the highest SVI values

for the study period as well as some of the highest precipitation amounts for the 31 days prior to collection, 42.7 and 87.2 mm, respectively. The low SVI values for the P class during the July collection at first appear anomalous, considering 69.1 mm of precipitation fell during the 31 days prior. However, considering the low precipitation amounts during the winter and spring months prior to July and that 28.9 mm of the 69.1 mm of the total monthly precipitation fell during the week immediately prior to collection, it is not surprising that piñon continued to display low photosynthetic activity comparable to the rate displayed in May. The lower greenness displayed by piñon when compared to juniper may be explained by the isohydric strategy of piñon to stop or greatly reduce photosynthesis in response to drought when compared to the anisohydric juniper which continue photosynthesizing in drier conditions (McDowell et al., 2008; Petrie et al. 2016).

3.1 Evaluation of Precipitation Preceding Landsat Imagery

Rainfall events of similar intensity to the 2015 May collection preceded each Landsat image collection date for the study period (Table 3). This moderate pre-monsoonal precipitation and relative evenness allowed for the greatest overall class separability between the primary scene components.

3.3 MESMA Evaluation

3.3.1 Accuracy Assessment

Statistical tests computed for fractional cover accuracy were based on high spatial resolution reference imagery. Statistical test results (RMSE, MAE, and R^2) from 2014 and 2015 are shown in Table 4. Accuracy assessment results from 2014 show a high degree of agreement between the modeled and reference fractions. Of all the classes modeled, the soil fraction had the lowest MAE and RMSE and the second highest R^2 value (Figure 12). The high agreement is not surprising given the contrast in spectral characteristics (e.g., higher reflectivity, spectral shape) of soil compared to the other cover types. NPV showed a similar level of agreement between modeled and reference fractions with low MAE and RMSE and a R^2 of 0.96. Evaluation of H and DP classes demonstrated a lower degree of accuracy between reference and modeled fractions in comparison to overall NPV. There was a high degree of agreement between reference and modeled fractions for GV (low MAE and RMSE), however, the R^2 value for GV (0.63) was relatively low compared to the other classes.

A comparison of reference and MESMA modeled fractional cover for 2015 showed a similar pattern of agreement to 2014 (Figure 12). Bare ground and NPV exhibited low MAE and RMSE with R^2 values of 0.95 and 0.96, respectively. GV endmembers continued to display a high degree of agreement between reference and modeled fractions (MAE=0.025 and RMSE=0.028), and a lower R^2 (0.74) value continued to typify the GV class.

3.3.2 Fractional Cover Estimates

Fractional cover was assessed quantitatively for the dominant land cover classes modeled across the DCP study region and for specific sites within the DCP. Maps illustrating fractional cover estimates for GV, NPV, and soil in the DCP are shown for each date (Figure 13). Maps illustrating fractional cover estimates for each endmember class (GV, NPV, and soil) were calculated for the DCP (Figure 14). Individual fractional cover estimates were calculated for each land cover class – P (Figure 15), J (Figure 15), DP (Figure 16), Soil (Figure 17), and H (Figure 18). Bar graphs illustrating fractional cover estimates for GV, NPV, and soil are shown in Figure 19 and target land cover classes (P, J, DP, H, and soil) are shown in Figure 20.

3.3.3 Temporal Changes in Fractional Cover

The distribution and stability of modeled fractions were evaluated with regards to expected changes in land cover classes following well understood disturbances that occurred during the study period. The most pronounced change in fractional cover occurred between GV (P and J) and NPV (H and DP), reflecting the extensive piñon die-off at the site. Across the entire DCP, from 2009-2015, GV declined from 32.7% in 2009 to 16.6% in 2015, an overall fractional cover decline of 16.1% (Table 5), with a peak GV fraction of 44.8% in 2011. This extensive reduction in GV coincided with an increase in NPV. Between 2009 and 2015, fractional NPV cover increased 21.4%. The proportion of NPV reached its lowest point in 2011 at 38.8%, during the same year when the proportion of GV peaked.

An assessment of the PJC and PJG sites within the DCP provided a way to assess how well MESMA modeled actual change in P, J, and DP. All mature piñon at the PJG site were girdled in September 2009. The effect of girdling was reflected in the MESMA results with a substantial decline in the proportion of GV. Decline in GV proportion at the PJG site occurred a year earlier than the DCP as a whole. Fractional GV cover declined 16.4% throughout the study period while NPV increased 20.4% at the PJG (Figure 19).

Field measurements at the site documented complete defoliation of girdled piñon trees by August of 2010 (Krofcheck et al. 2014). MESMA fractional cover estimates for the PJG showed a 20.7% decline of GV between 2010 and 2011, corresponding to the defoliation date (Table 5). Complete defoliation of girdled piñon trees coincided with a sharp increase in the proportion of NPV between 2010 and 2011 (16.4%). GV fraction declined 30.9% from a pre-girdle high of 46.4% in 2010 to a study period low of 16.6% in 2015. This decline occurred coincident to a 36.8% increase of NPV over the same time period.

The change in fractional cover proportions at the PJC are similar in timing to the change in proportion for the entire DCP. At the PJC, GV declined 13% across the study period from 31.7% in 2009 to 18.7% in 2015 (Table 5). GV declined from a peak proportion of 49.4% in 2011 to a study period low of 18.7% in 2015. Like the PJG, the extensive reduction in GV occurred commensurate with an increase in NPV. Between 2009 and 2015, NPV increased 22.4% at PJC. The lowest overall NPV proportion at the site was 40.2% in 2011. The NPV proportion then increased 40.1% in the following three years to a high of 82.3% of cover in 2015 (Table 5).

Change in soil across all sites displayed a similar pattern. In the year immediately following the initial decline in GV (DCP-2011, PJG-2010, and PJC-2011) the proportion of soil peaked and then experienced a steady decline in the following years (Figure 19). Peak soil proportions coincided with the driest years (2010-2011) in the study period when herbaceous cover was least active.

Intra-endmember class (P and J, and DP and H) fractional cover demonstrated considerable variation throughout the site and across the study period. Across all sites, the proportion of H remained a small component of the landscape, changing little across the study period. Within the NPV class, the percentage of dead piñon (DP) across the DCP increased from 50.7% in 2009 to 74.5% in 2015. At the PJC and PJG, the overall percentage of DP increased 21% and 26.4%, respectively (Table 6). The proportion of DP at PJG increased sharply between 2010 and 2011, a year earlier than both the DCP and PJC, coinciding with the defoliation of girdled piñon . Across the DCP, PJC and PJG, the increase in DP coincided with a decrease in P, indicating the ability of MESMA to accurately model P mortality as an increase in DP (Figure 20).

3.4 Change in Piñon and Juniper Abundance

MESMA model variation used in the unmixing process indicate species specific fractional cover is discernable between P and J. A trend towards decreasing piñon was observed across the DCP. This decline was mirrored by a nearly equivalent increase in DP across the study period. Analysis of annual changes in class proportion and model selection indicate that P and J are spectrally separable in Landsat using MESMA.

Fractional cover results indicate a 24.5% decline in P from 29.2% in 2009 to 2.2% in 2015 across the DCP (Table 6). The decline at the PJG was even more pronounced, with the proportion of P falling 32% from 34.2% in 2009 to 2.2% in 2015. While there was a slight increase in P fractional cover between 2009 and 2011, the proportion of P showed a general trend of decline in cover across the study period.

Between 2009 and 2015 the juniper fraction increased in contrast to the decline in P across the DCP (Figure 20). Across the study period, the proportion of J increased from 6% in 2009 to 11.9% in 2015 of total fractional cover across the DCP. A similar trend was seen at the PJG and PJC. However, this trend is likely attributable to herbaceous green up under dead piñon canopies, discussed in further detail below in the discussion section.

An evaluation of fractional cover changes at the PJC shows similarities to the DCP as a whole. Complete defoliation of girdled piñon occurred at the PJG between 2010 and 2011. Over the same time period, the proportion of P declined from a study period high of 43.3% in 2010 to 27.6% in 2011 (Table 6). This decrease contrasts with a moderate increase in P across the ungirdled DCP and PJC over the same period, reflecting that the site was not girdled. However, across the study period, the proportion of P declined from 23.2% in 2009 to 0% in 2015 at the PJC. A significant decrease in P fractional cover following piñon girdling at the PJC commensurate with relatively stable J fractional cover indicates the ability of MESMA to detect spectral changes unique to individual P and J classes.

As P mortality spread across the site, the date of mortality onset at individual sites is detectable. P proportion increased across the DCP between 2009 and 2011 to a high of

44.6% in 2011 then sharply declined to 17.9% in 2013 (Figure 20). Similar to the DCP, the onset of P mortality at the PJC occurred between 2011 and 2013 where P declined from a study period high of 50.7% in 2011 to 3% by 2013. The timing of P decline at the ungirdled DCP and PJC indicate widespread P mortality occurred between 2011 and 2013.

Chapter 4

Discussion and Conclusions

4.0 Discussion and Conclusions

Rapid climatic transition is forecast for the Southwestern U.S. with higher temperatures and less precipitation predicted to continue for the next 100 years (Seager et al., 2012; Overpeck & Udall, 2010). To mitigate the potential widespread deleterious impact of such rapid change, effective strategies must be in place for monitoring how PJ woodlands react to a warmer, drier environment. Previous studies have demonstrated the applicability of remote sensing technologies in monitoring PJ woodlands (e.g., Krofcheck et al. 2014). This thesis expands on those studies by showing that in-situ spectral data and MESMA can successfully be used for measuring vegetation change in PJ woodlands replicable regionally on an annual time-scale.

In-situ spectral measurements collected throughout a growing season and generation of spectral vegetation indices allowed for the identification of the ideal phenological phases to separate the primary land-cover types present in a PJ Woodland at the Deer Creek Plateau, New Mexico. High spectral resolution field spectroscopic data collected at five points evenly spaced throughout 2015 were shown to be useful for determining when P and J were most separable from surrounding vegetation and from each other.

For 2015, early summer (May) was the ideal date of separability between all classes. At this period in the growing season, P and J are most separable from one another and the other dominant land cover types. P and J showed different phenology in response

to the warmer temperatures and drier conditions found during early summer, with P showing lower NDVI values than the more stable J. Herbaceous vegetation has greened up in response to precipitation and warmer temperatures, allowing for sufficient separation from DP and soil, though the photosynthetic response of Herbaceous cover is still less than P and J, allowing for spectral distinction. Inter-annual variation in precipitation may affect the onset and duration of phenological changes, and consequently the optimal dates of discrimination, yet this exploration provides insight into the spectral-temporal characteristics of the dominant land cover components of piñon-juniper woodland.

Scene vegetation components showed significant variation related to the onset and duration of the summer monsoon (late June-August), with greatest separability occurring immediately before the onset of the monsoon season. This suggests the timing of image acquisition prior to major precipitation events is critical for effective separation of semi-arid vegetation cover types in remotely sensed imagery. Image selection for this study was limited to a +/- 2 week window around the May 7th separability date and could have been improved with a more thorough review of precipitation records. Examining the time since last major precipitation event and total weekly/monthly precipitation prior to image collection could help minimize the effects inter-annual precipitation variation on vegetation phenology. Selecting images with minimal inter-annual variation in precipitation prior to image collection is more essential for reducing inter-annual variability in green-up than just limiting the selection of images to +/- 2 weeks of May 7th.

However, the findings from this research indicate that MESMA applied to a Landsat time series is capable of distinguishing between the primary land-cover components of a piñon-juniper woodland with a high degree of accuracy. MAE and RMSE values were below 0.05 for all modeled and reference percentages at both accuracy assessment dates, indicating that MESMA is effective at quantifying changes in fractional cover above 0.05, providing a way to accurately quantify fine shifts in vegetation abundance.

MESMA was able to reliably quantify fractional changes in P cover; demonstrated in this study by modeling the decrease in P with a proportional increase in DP post mortality across the DCP. Assessment of fractional cover proportions at the PJG provided an additional opportunity to assess the potential of MESMA to model species level vegetation changes in an artificially disturbed environment. Modeled fractional cover changes were analogous to expected changes in vegetation cover at the DCP and to measurements of primary land-cover components estimated using high spatial resolution imagery acquired in 2014 and 2015.

MESMA results from Landsat time series showed a decline in P fractional cover at all three sites, consistent with observed widespread P die-off. Between 2009 and 2015, total fractional cover of P decreased from 29.2% to 4.7% across the DCP, demonstrating the sensitivity of MESMA to detecting the decline in P abundance. In addition, across the DCP as a whole, the 24.5% decline in total fractional cover of P throughout the study period closely matched a near proportional 23.8% increase in total fractional cover of DP. At the smaller PJC, MESMA modelled a 23.2% decline in the total fractional cover of P with a nearly proportional 21% increase in the total fractional cover of DP. Similarly at

the PJG, P declined 32% in total fractional cover while DP increased 26.4%, further indicating the ability of MESMA to model the transition of P to DP post mortality.

However, it is unknown how well MESMA was able to classify P in the process of dying. Prior to mortality, the trees become chlorotic when their leaves are unable to maintain normal chlorophyll levels due to stress. The spectral signature of chlorotic trees likely differs from a healthy (nonchlorotic) and defoliated tree. However, the transition between a live and dead tree during which a tree is chlorotic is brief. Therefore while it is possible that enough trees experienced chlorosis simultaneously across the plateau to affect fractional cover results during a few study years, since fractional cover of P in 2009 was determined pre-drought when trees were mostly healthy, and post-drought in 2015 when trees were either completely defoliated or mostly nonchlorotic, estimated total fractional cover change for P across the study period was likely not seriously affected.

In spite of chlorotic events, MESMA fractional cover results showed continuity across the P and DP classes, fractional cover for the J class showed significant variation across the study period at all sites. For example, at the DCP total fractional cover of J increased from 6% to 11.9% between 2009 and 2015. This increase is unlikely for the slow growing woody juniper during a drought period. The increase is likely attributable to inter-annual fluctuations in herbaceous cover misclassified as J. Previous studies have shown herbaceous cover to increase in abundance underneath the canopies of defoliated piñon trees post mortality (Krofcheck et al., 2014). It is likely that this increase in herbaceous cover is responsible for the increase in J fractional cover during the study period. Collecting spectra for these mostly annual herbaceous species for inclusion in the

unmixing process would help reduce erroneous fluctuations and misclassification in the J class.

Overall, MESMA demonstrated an ability to distinguish and map stress-induced physical changes in a PJ Woodland. As drought is predicted to increase in intensity and frequency for the immediate future in the Southwest United States, forest mortality is likely to continue (Breshears et al, 2009; Williams et al, 2013; IPCC, 2014). Vulnerable species like piñon pine will be the first to show the effects of stress, a key indicator species for climate related disturbance. MESMA has been proven to be a valuable tool for mapping and monitoring species level changes in piñon-juniper woodland.

4.1 Limitations of Study

Due the launch failure of Landsat 6 and the scan line corrector (SLC) failure aboard Landsat 7, complete Landsat data is unavailable for 2012. Normal data infills for Landsat 7 images with the SLC off will not account for the data accuracy needed for MESMA analysis. Therefore, 2012 was a permanent gap year in the study.

All imagery was selected for clear atmospheric conditions with reference to precipitation records. However, the need to use cloud free scenes in the analysis introduced a temporal offset in the study period equal to one month between the earliest scene date (April 22nd) and latest date (May 21st). Inter-annual variation in vegetation phenology due to precipitation and temperature likely increased due to this temporal offset, influencing the fractional cover.

Landsat scenes are geometrically corrected to a level L1 T standard. Little variation in pixel placement exists for the same Landsat scene date-to-date. However, it is impossible to determine small co-registration errors between the Landsat images and the higher-resolution images used in the accuracy assessment. Large co-registration errors (where present) were detected and corrected using a second order polynomial warp, but errors smaller than 30 meters are difficult to detect and are, therefore, permanent. The effect of this error on results was reduced by enlarging the accuracy assessment area to a 3 x 3 pixel area, but some co-registration error must be accepted as part of this study.

Temporal mismatch in the collection of the accuracy assessment and Landsat imagery also likely introduced small levels of error in the accuracy assessment results. Vegetation in the accuracy assessment imagery collected in October looks different than the vegetation classified in the May Landsat dates due to seasonal differences in precipitation. That difference likely introduced small levels of error in how that vegetation was classified in the accuracy assessment. In addition, the five month temporal difference of the two imagery collection dates likely introduced a temporal mismatch between visible changes in system structure due to the widespread P dieoff. This effect likely caused P mortality to be slightly overestimated in the accuracy assessment imagery.

In addition, mapping spectrally diverse PJ semi-arid woodland is challenging due to the heterogeneous mixture of perennial and annual grasses and forbs as well as evergreen conifers. Collecting additional spectra for inclusion in the spectral library would add rigor to the unmixing process. Adding spectra for the annual forbs that grow underneath defoliated piñon canopies, in particular would help reduce misclassification

in the J class. Additional site planning during summer would be necessary to identify the location and variety of herbaceous cover present at the site that senesce post monsoon.

Finally, a stand of ponderosa pine (*Pinus ponderosa*) went unnoticed on the plateau during spectra collection. MESMA overclassified the abundance of P for that section of the plateau due to the lack of spectral information for the grove (Figure 14). Adding spectra for ponderosa from either in-situ data or a previously created spectral library would help to correctly classify the grove, further reducing misclassification. In conclusion, building a spectral library that more appropriately describes the heterogeneous land cover present at the site would do the most to improve future MESMA classification results.

4.2 Future Research

This research would benefit from the addition of more spectra collections throughout the year. Spectra collections made at monthly intervals would provide additional information about species-specific phenophases and the relationship to seasonal precipitation patterns. These collections would potentially allow the identification of a date with greater separability. The inclusion of more spectra collection sites representative of component materials (ie. soil and herbaceous/grass) would aid in building a stronger model. The Deer Creek Plateau has a significant variety of herbaceous and graminoid species. The identification and inclusion of those species in the model would add robustness. Additional in-class endmember refinement within MESMA to

increase the separability of spectra used to model principle scene components would help strengthen results.

Incorporating additional PJ woodlands with distinct environmental characteristics and histories would provide an additional backdrop for future analysis. Examination of burned areas and woodlands closer to ecotone boundaries would further test the ability of MESMA to discern changes in PJ woodland cover. Expanding the study area to include the neighboring Sevilleta Longterm Ecological Research Station (SLTER) and Manzano Mountains offer that backdrop. The SLTER would incorporate a varied ecological gradient encompassing the lower elevation PJ ecotone while the Manzano Mountains would encompass the higher elevation PJ ecotone. In addition, the Manzano Mountains would provide a study area with varied wildfire histories affecting PJ woodlands. The study area expansion into these PJ woodlands would incorporate additional environmental characteristics that have been shaped by drought and climate change further testing MESMA's ability to model PJ woodlands with varied growth histories at a regional scale.

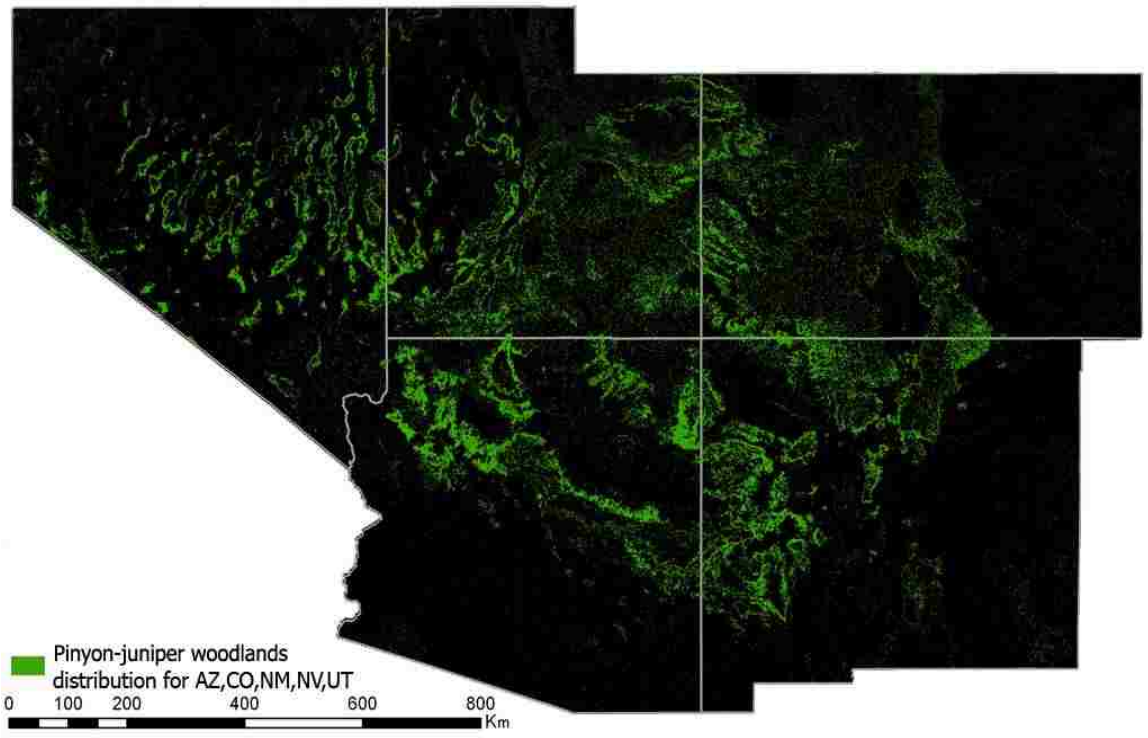

Figure 1. Piñon-Juniper range across the southwestern United States. Courtesy of: Pinyon Juniper Woodlands Information Network, 2004.

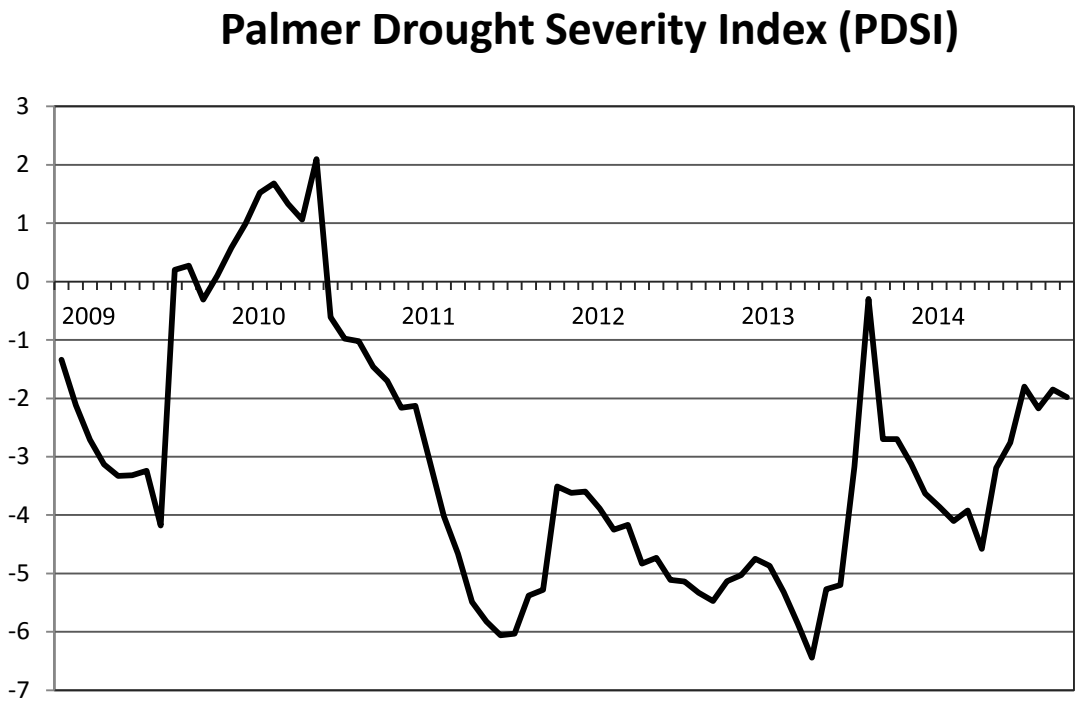

Figure 2. Palmer Drought Severity Index for the Middle Rio Grande Basin 2009-2014. Brewer, 2015.

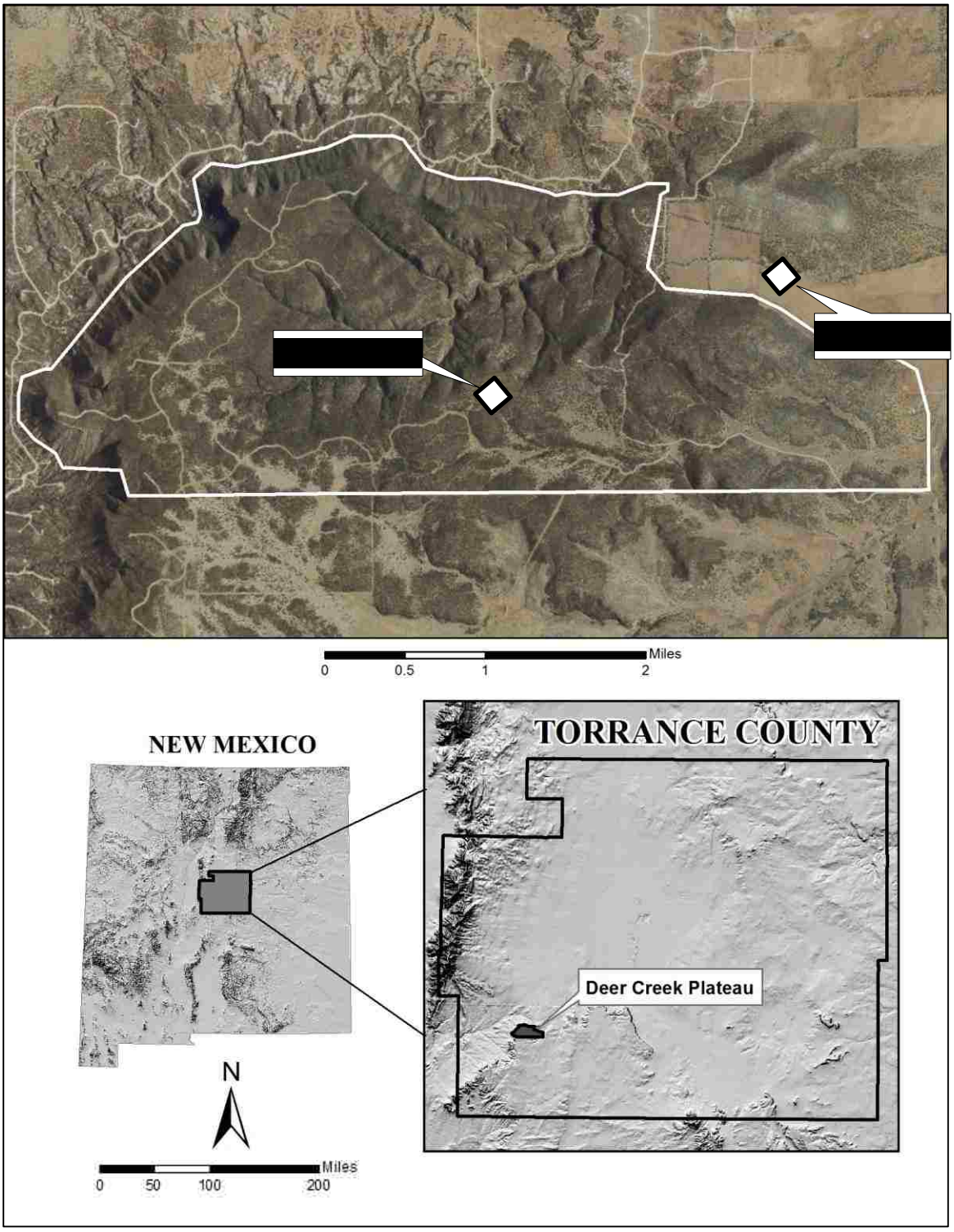

Figure 3. Deer Creek Plateau (DCP) study area outlined in white and PJ-Control (PJC) and PJ-Girdle (PJG) outlined in black.

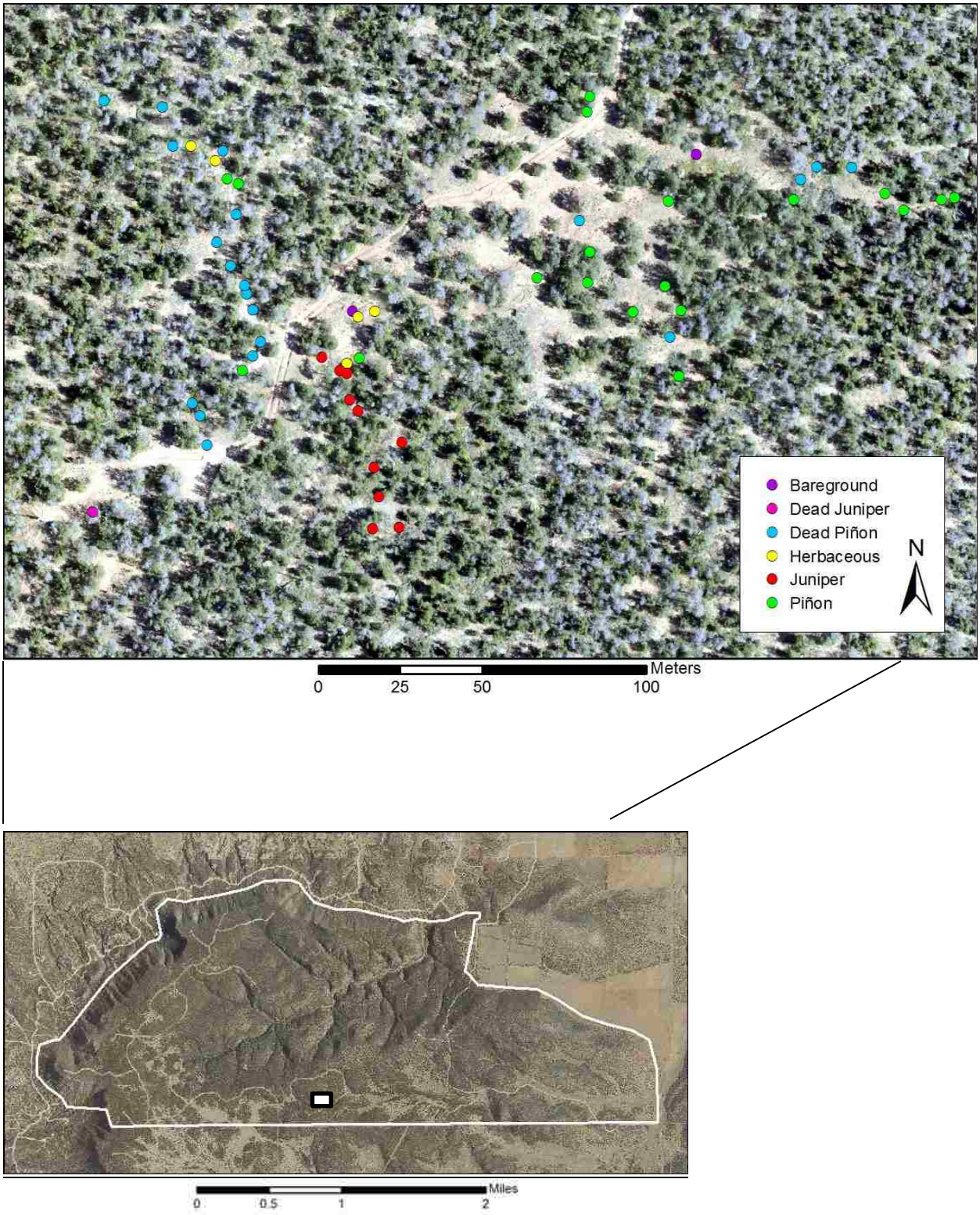

Figure 4. Field site locations.

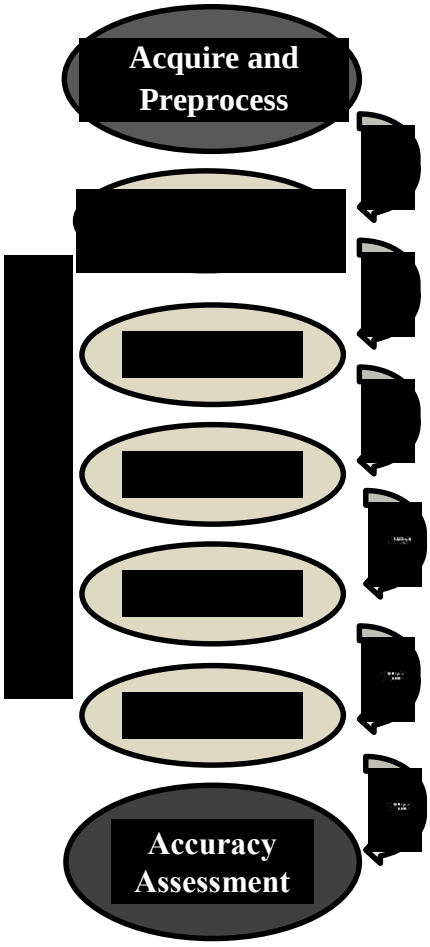

Figure 5. MESMA Workflow.

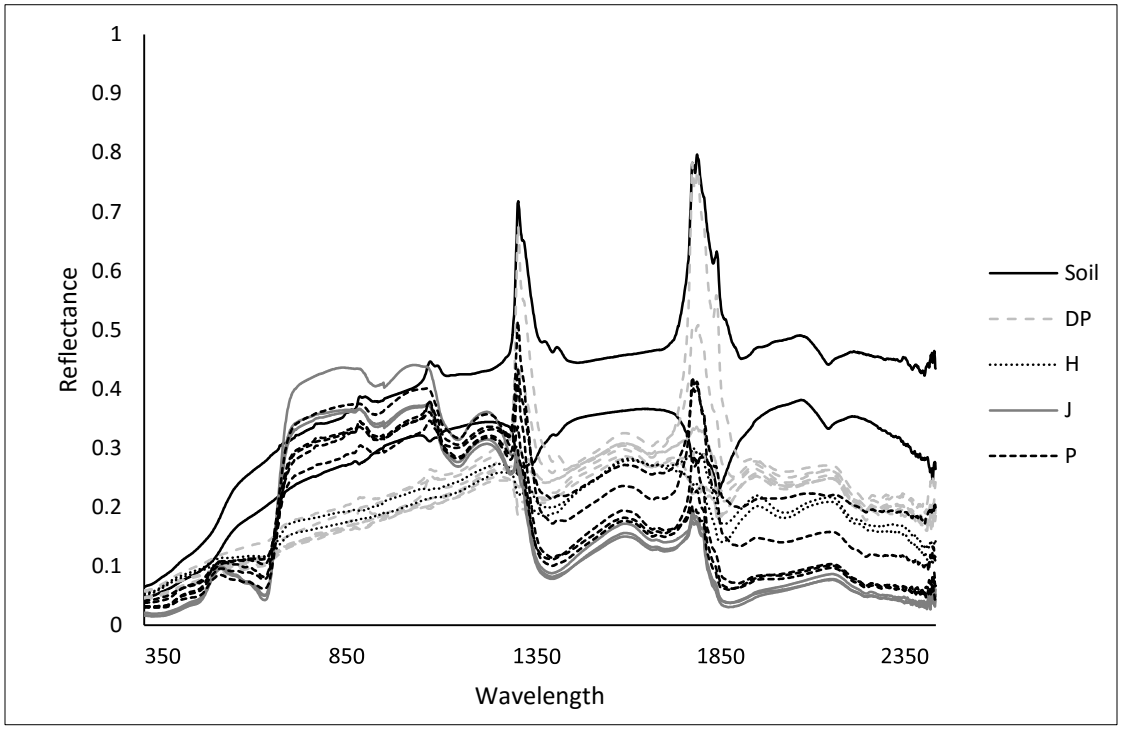

Figure 6. Reflectance curves for all selected spectra in May 7th collection date (n=19).

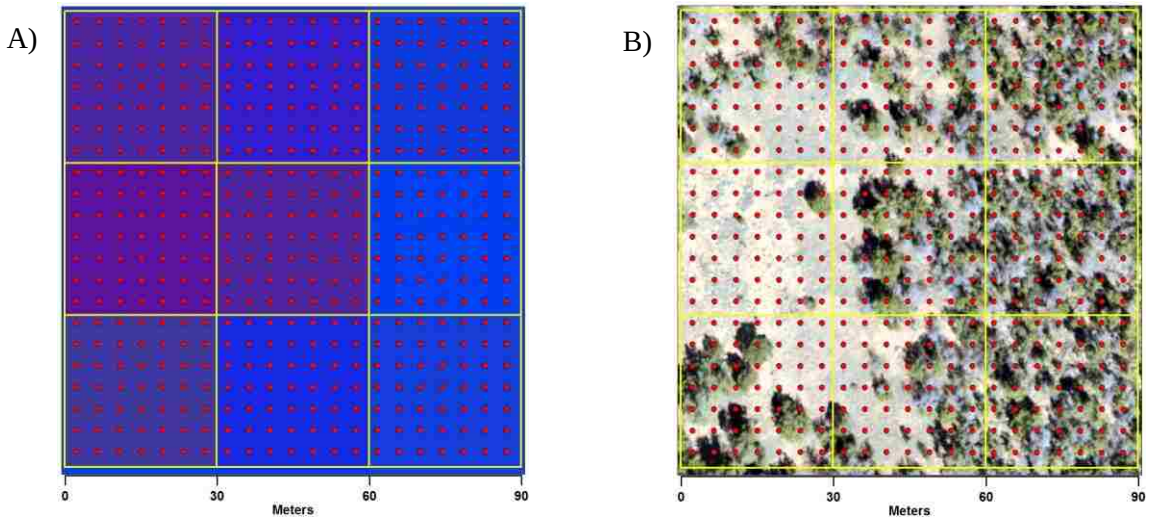

Figure 7. Example accuracy assessment plot where A) is a 90 x 90 m plot (9 Landsat pixels) overlayed by 450 sampling points. B) contains accuracy assessment imagery.

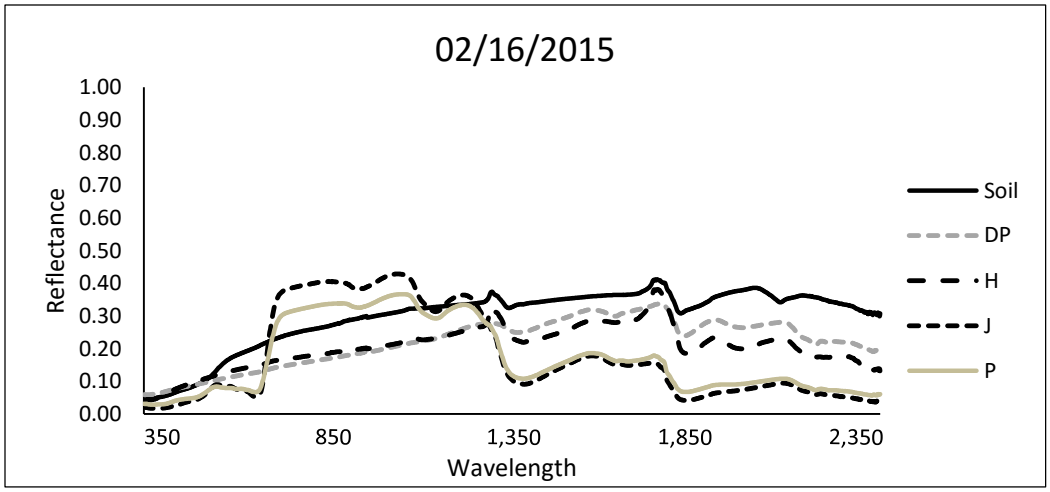
02/16/2015
Reflectance
1.00
0.90
0.80
0.70
0.60
0.50
0.40
0.30
0.20
0.10
0.00
350
850
1,350
1,850
2,350
Wavelength
Soil
DP
H
J
P

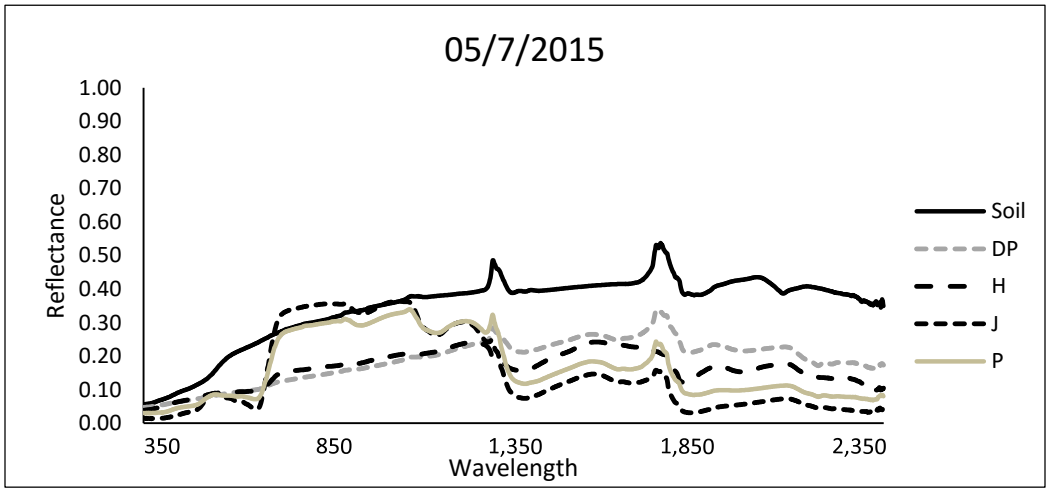
05/7/2015
Reflectance
1.00
0.90
0.80
0.70
0.60
0.50
0.40
0.30
0.20
0.10
0.00
350
850
1,350
1,850
2,350
Wavelength
Soil
DP
H
J
P

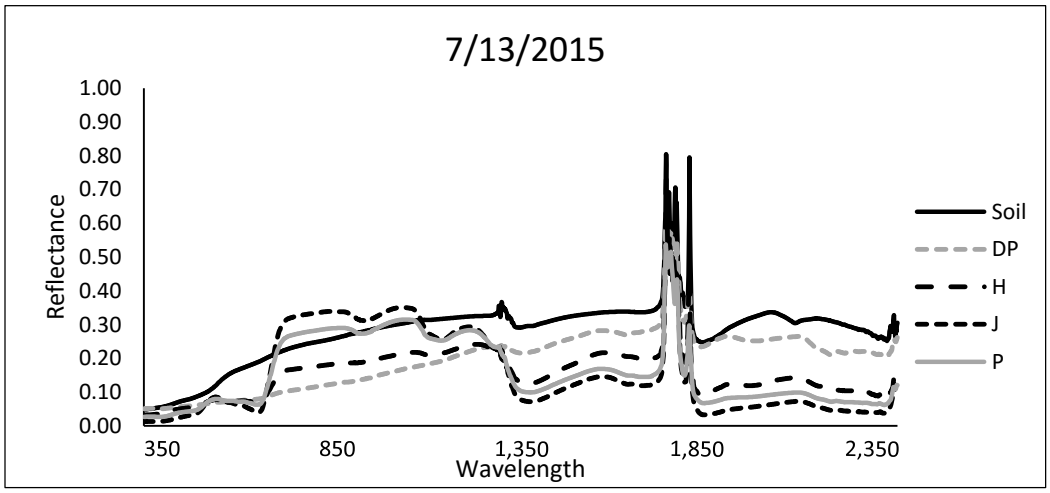
7/13/2015
Reflectance
1.00
0.90
0.80
0.70
0.60
0.50
0.40
0.30
0.20
0.10
0.00
350
850
1,350
1,850
2,350
Wavelength
Soil
DP
H
J
P

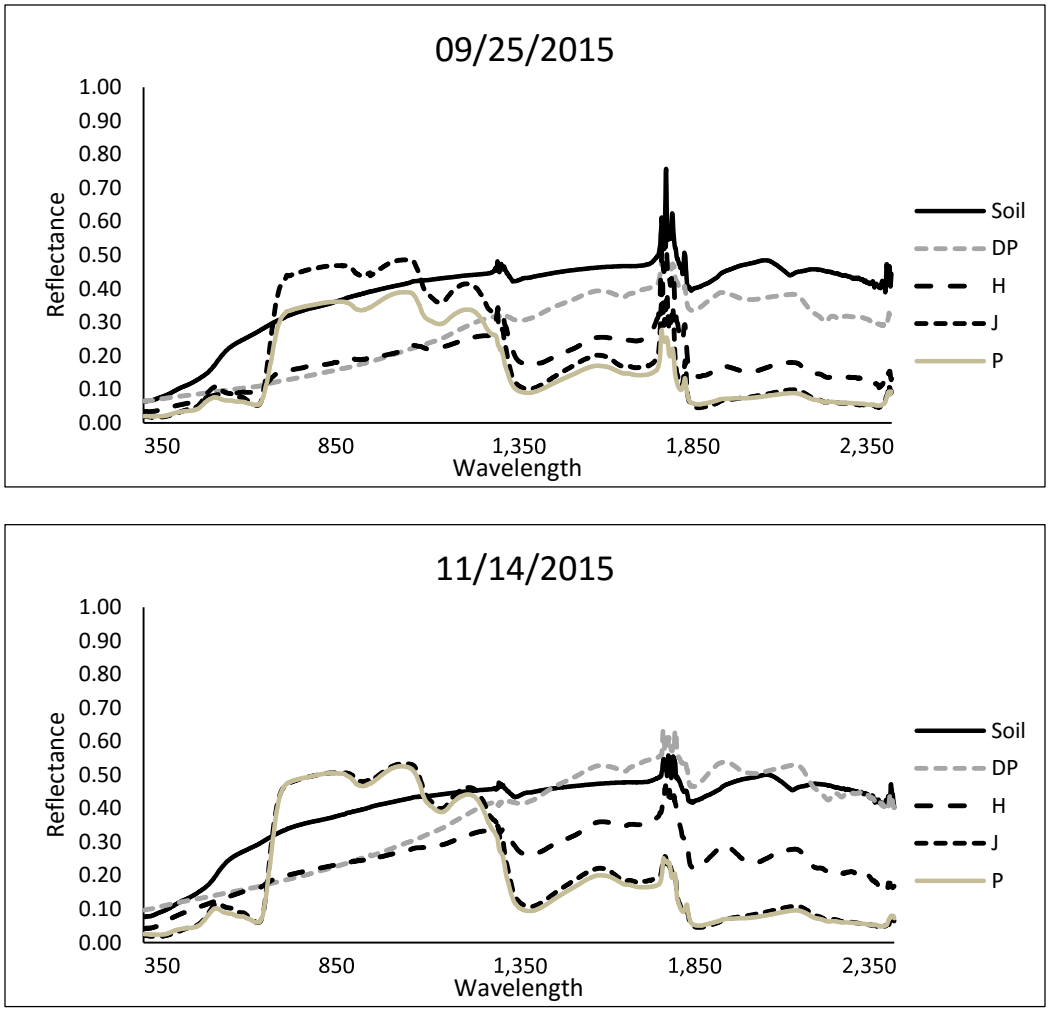

Figure 8. Mean spectral curves of spectra classes (Soil, DP, H, J, and P) at each collection date (February, May, June, September, November).

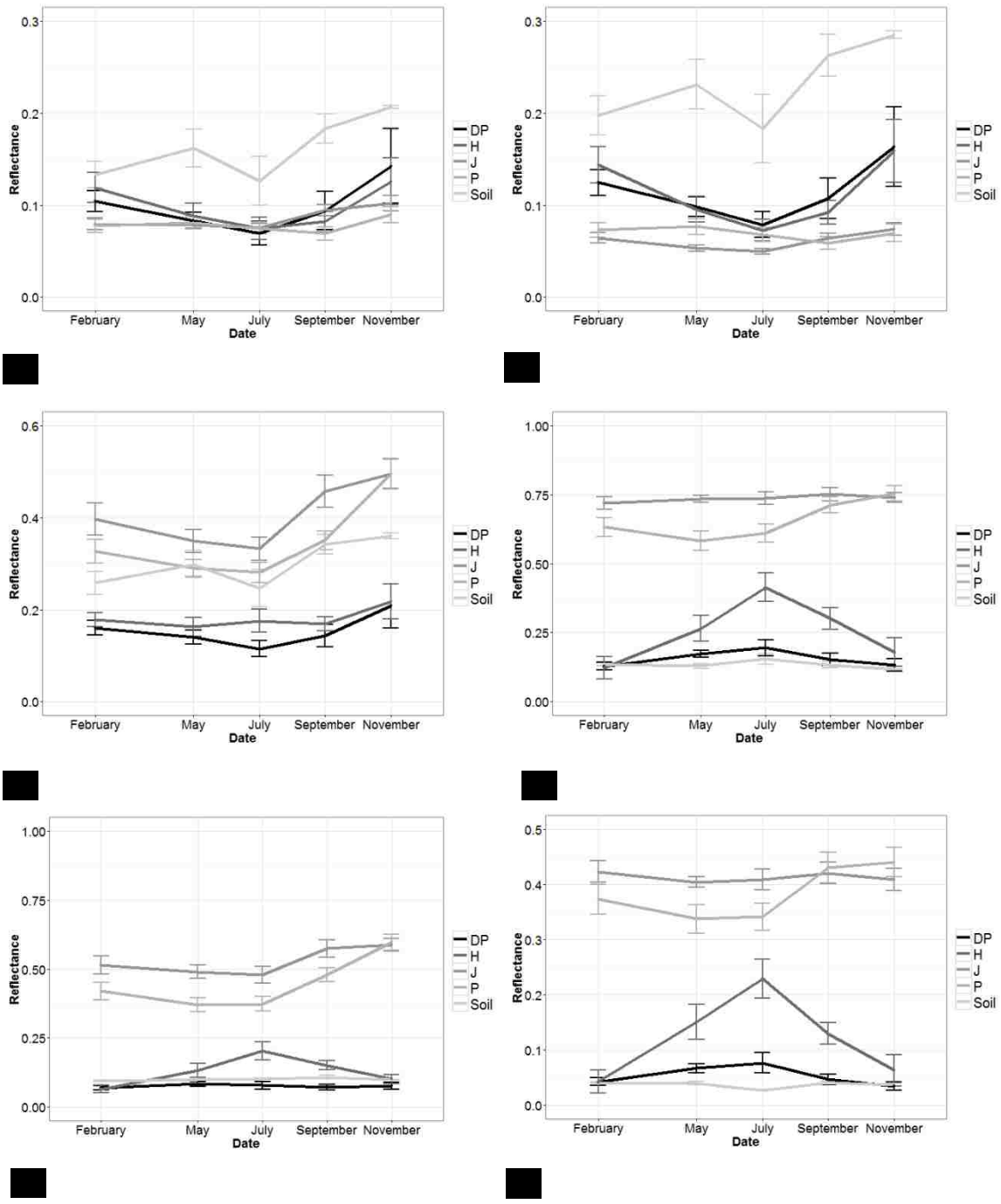

Figure 9. Reflectance spectra of all five cover type classes convolved to Landsat 5 TM a) Green, b) Red, and c) NIR bands, and broadband vegetation indices d) Normalized Difference Vegetation Index and e) Soil Adjusted Vegetation Index, and narrowband vegetation index f) Red Edge Normalized Difference Vegetation Index each with error bars (σ=1) per class.

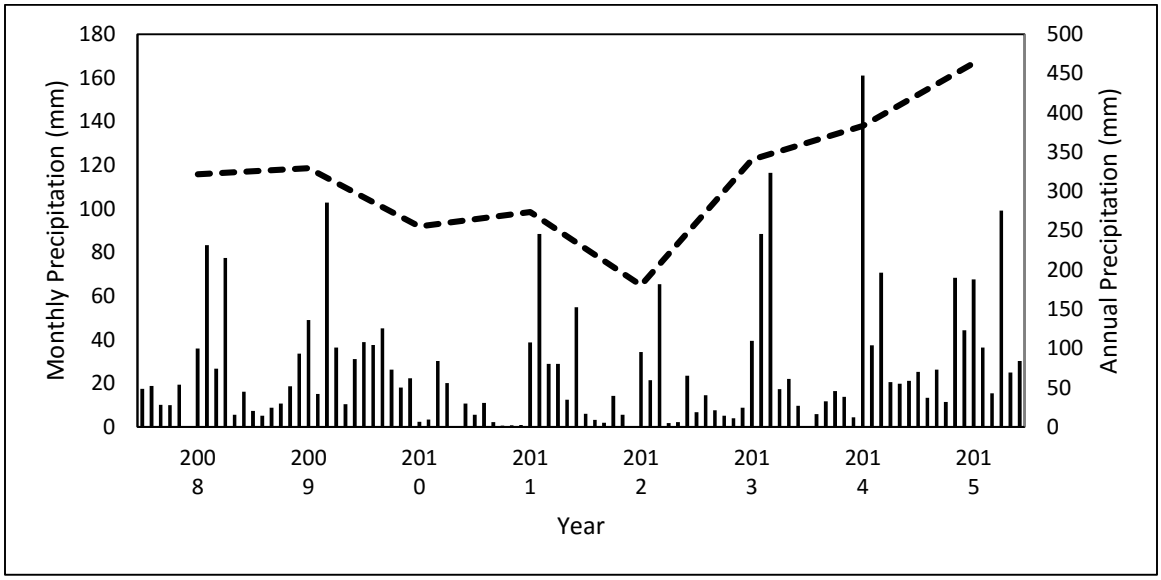

Figure 10. Total monthly and annual precipitation records from 2008-2015. Monthly precipitation shown in barplots and annual precipitation shown with dashed line.

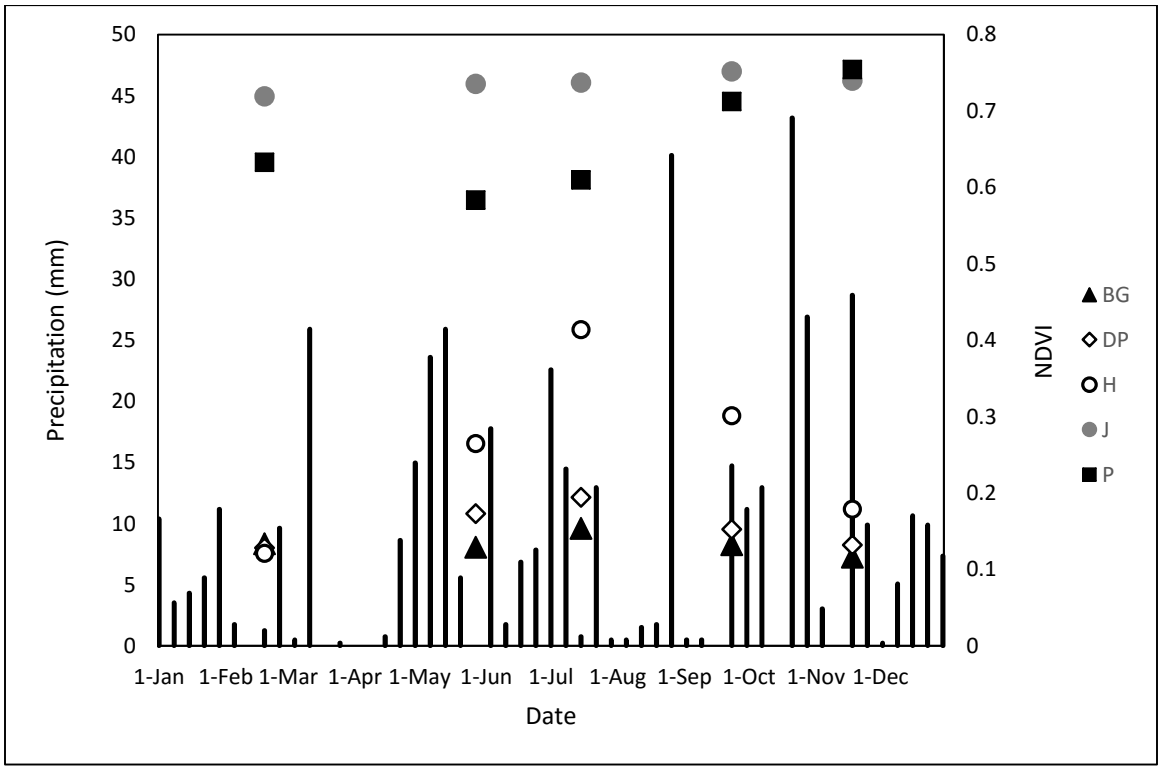

Figure 11. Weekly precipitation averages plotted against NDVI calculations of the five cover type classes for all five collection dates for 2015.

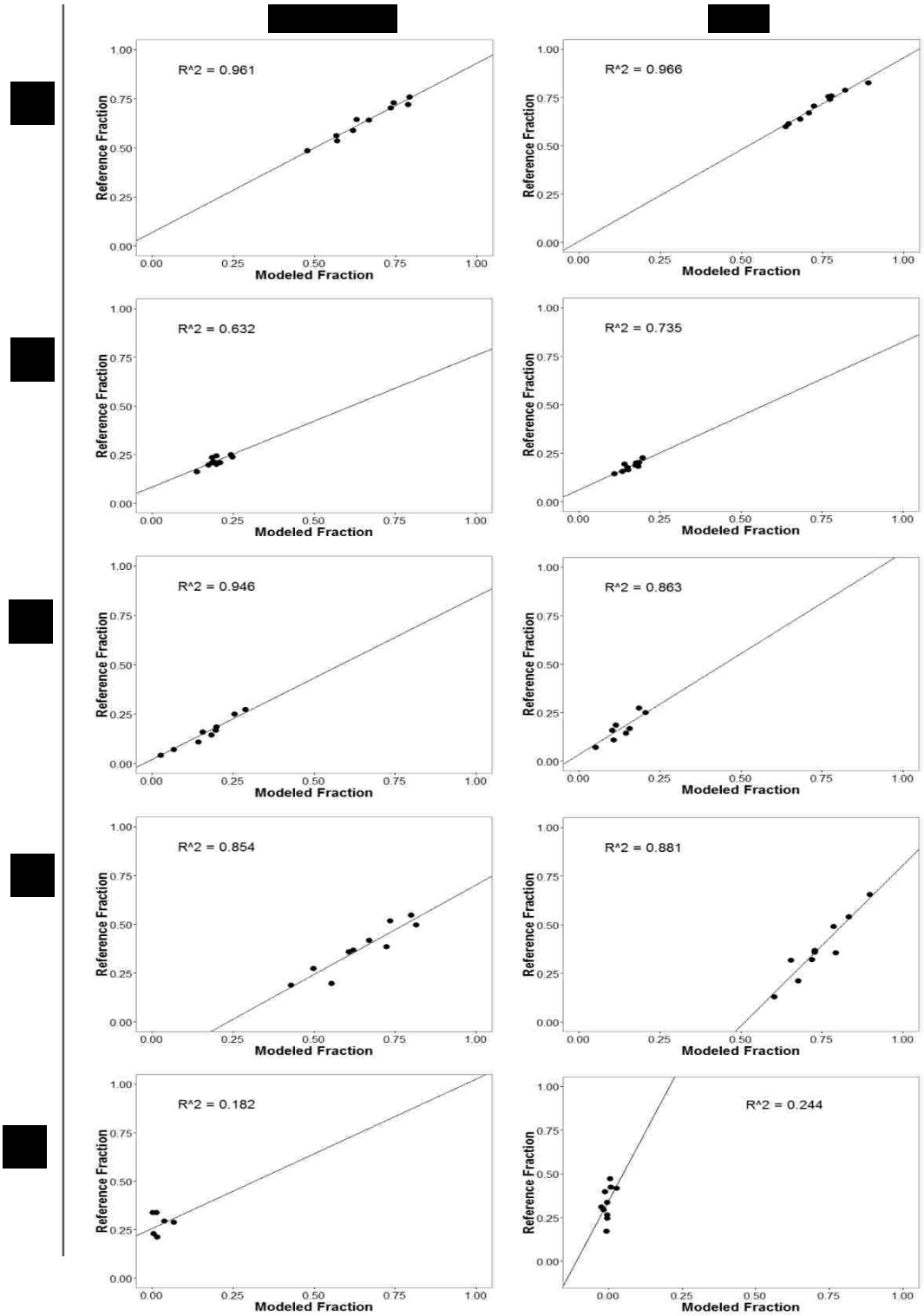

Figure 12. Regression models of modeled and reference fractions at each date for: Non-photosynthetic Vegetation (NPV), Green Vegetation (GV), Soil, Dead Piñon (DP), and Herbaceous (H).

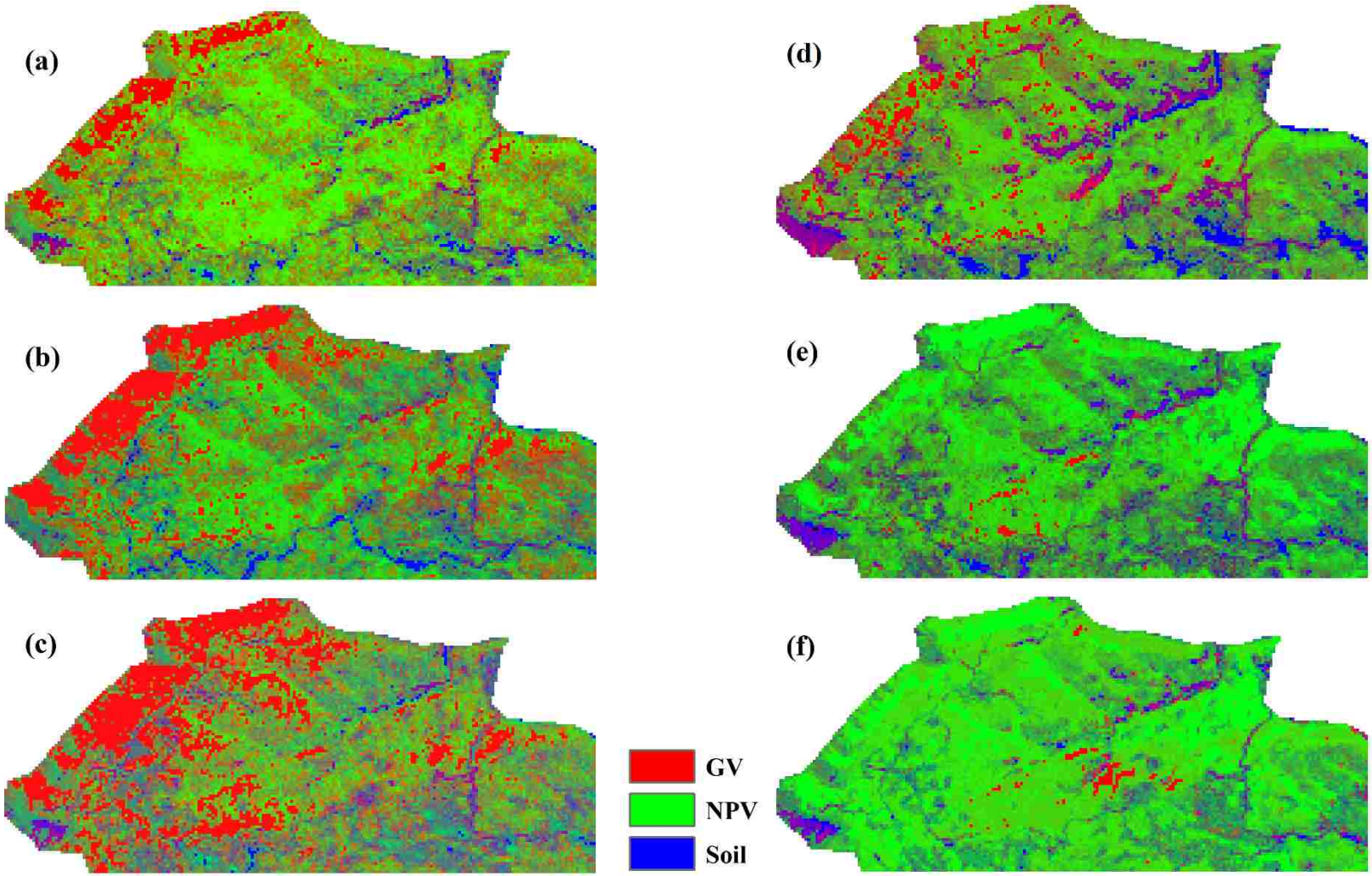

Figure 13. Fractional cover maps generated from MESMA results. GV, NPV, Soil are shown in RGB, respectively: a) 2009, b) 2010, c) 2011, d) 2013, e) 2014, and f) 2015. Color mixtures represent mixed fractional cover.

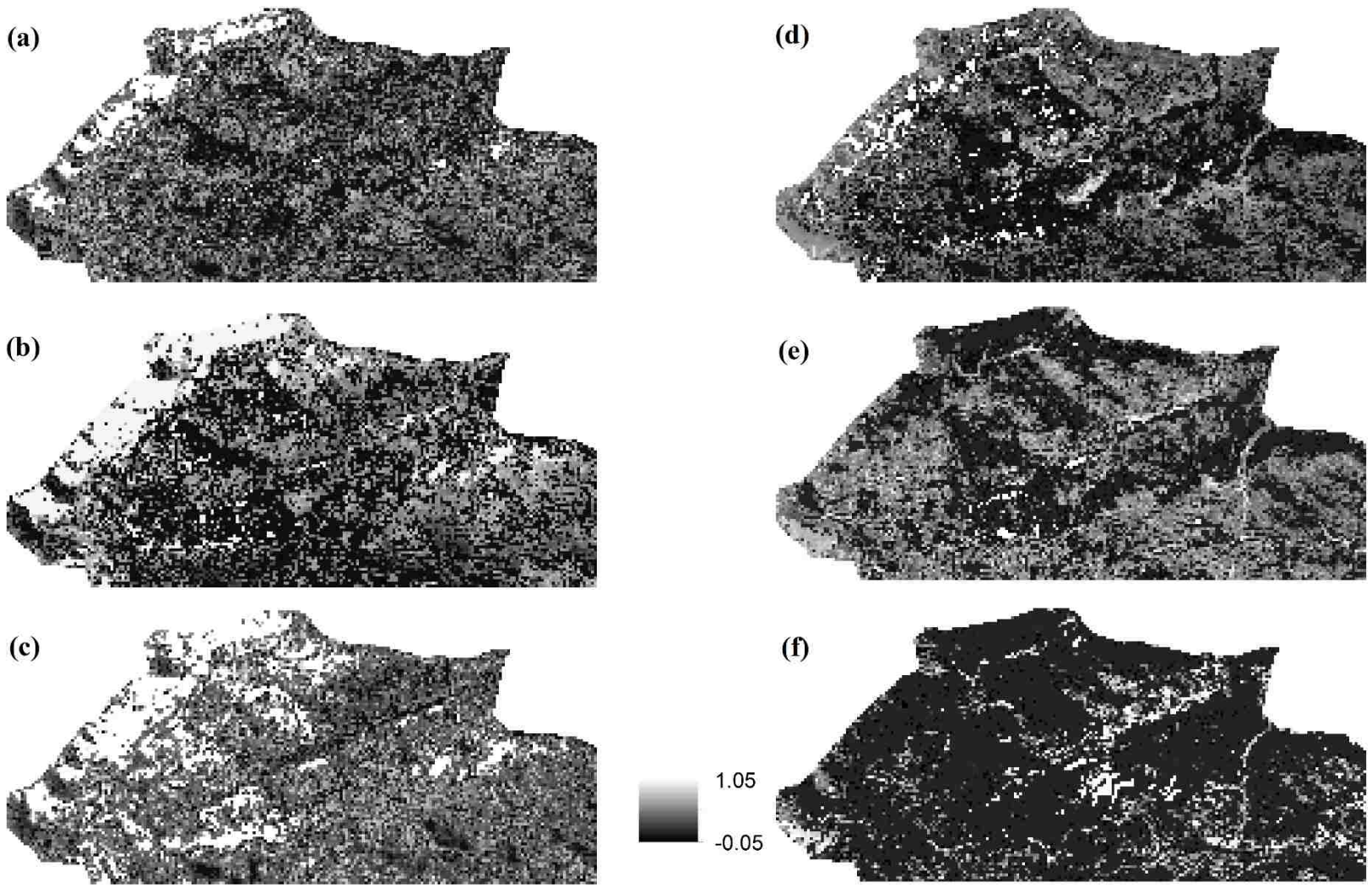

Figure 14. MESMA P proportions displayed in a stretched greyscale palette: a) 2009, b) 2010, c) 2011, d) 2013, e) 2014, f) 2015. Lighter tones represent higher P proportion, darker tones lower P proportion.

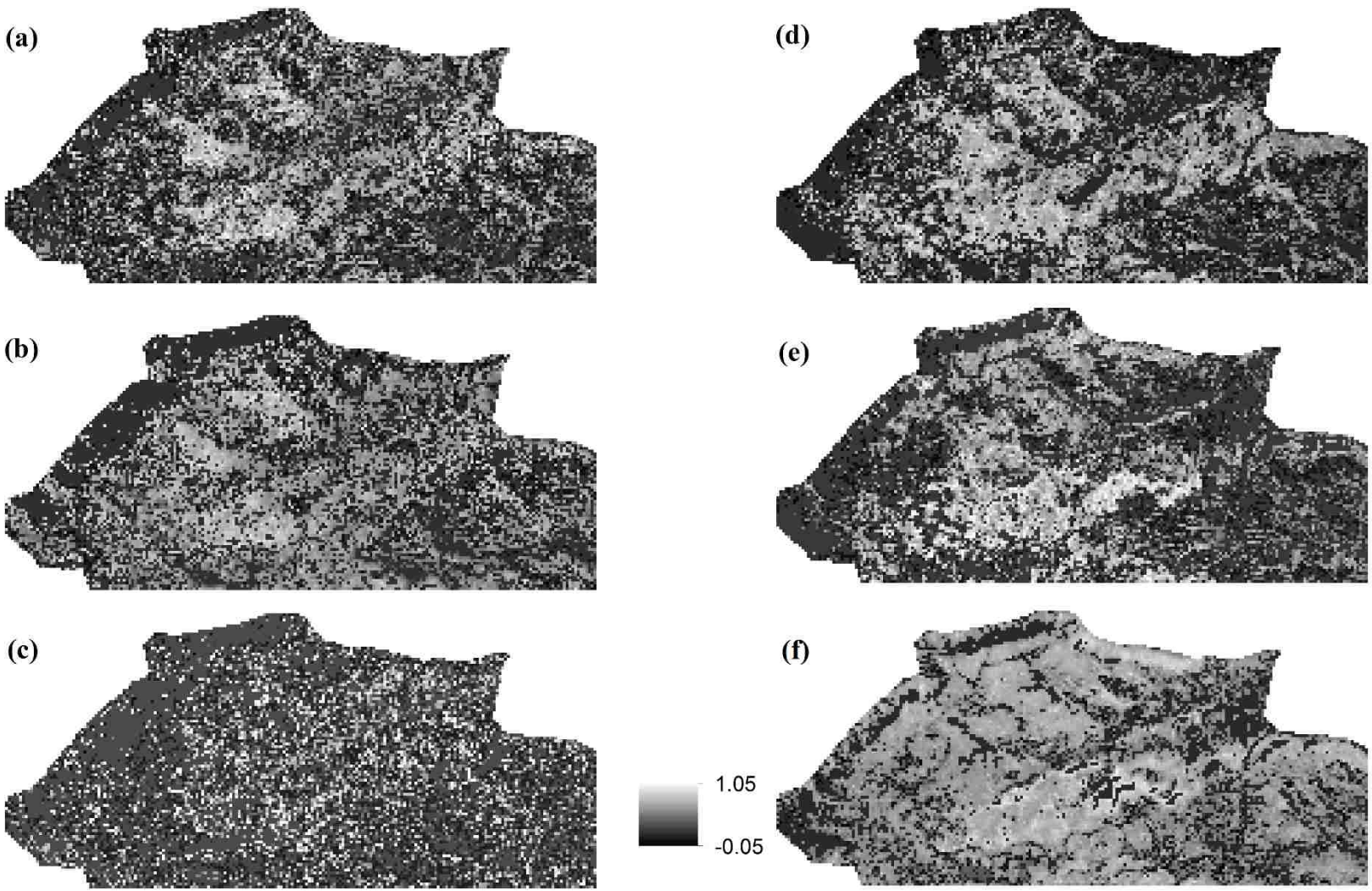

Figure 15. MESMA J proportions displayed in a stretched greyscale palette: a) 2009, b) 2010, c) 2011, d) 2013, e) 2014, f) 2015. Lighter tones represent higher J proportion, darker tones lower J proportion.

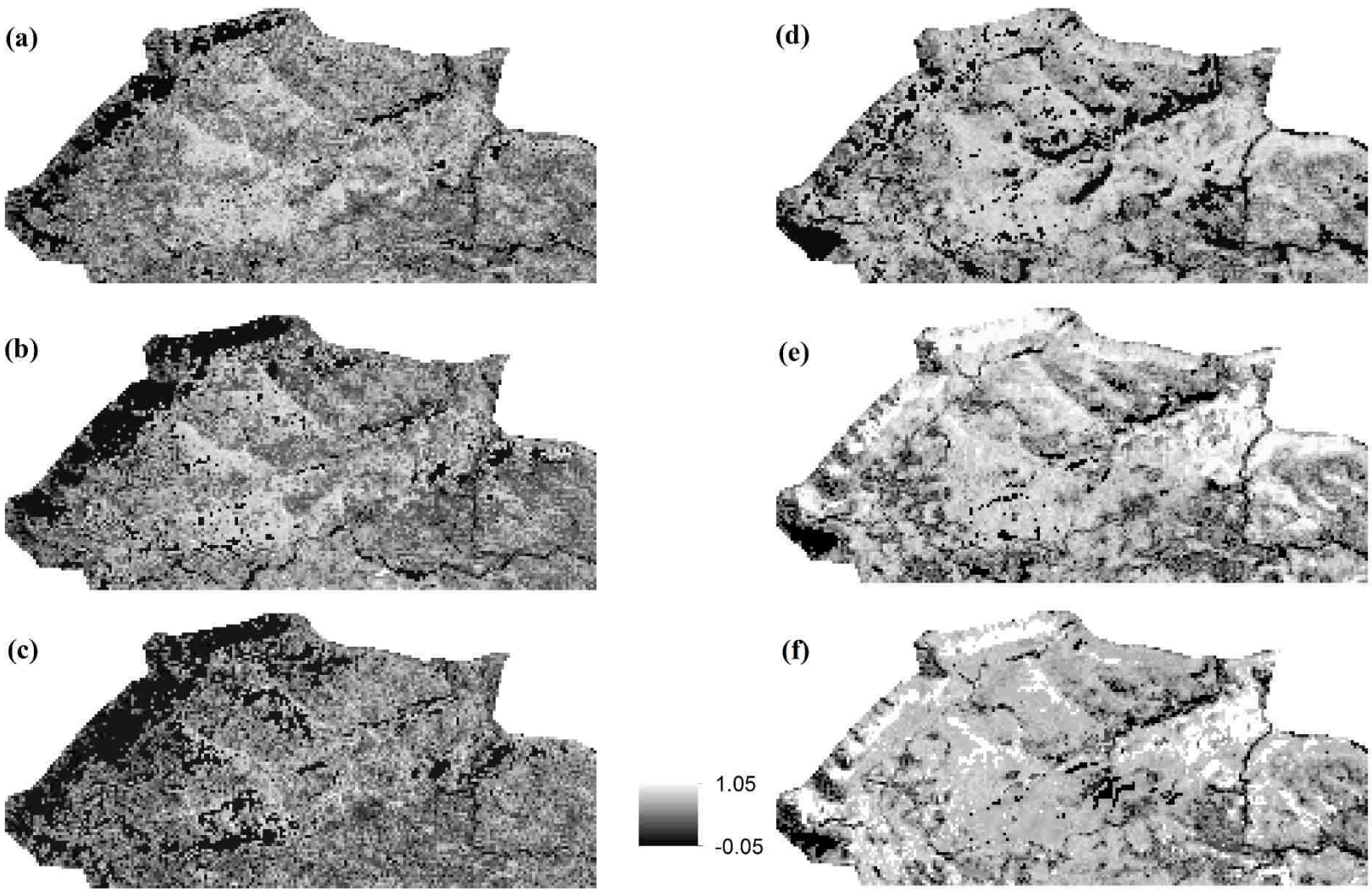

Figure 16. MESMA DP proportions displayed in a stretched greyscale palette: a) 2009, b) 2010, c) 2011, d) 2013, e) 2014, f) 2015. Lighter tones represent higher DP proportion, darker tones lower DP proportion.

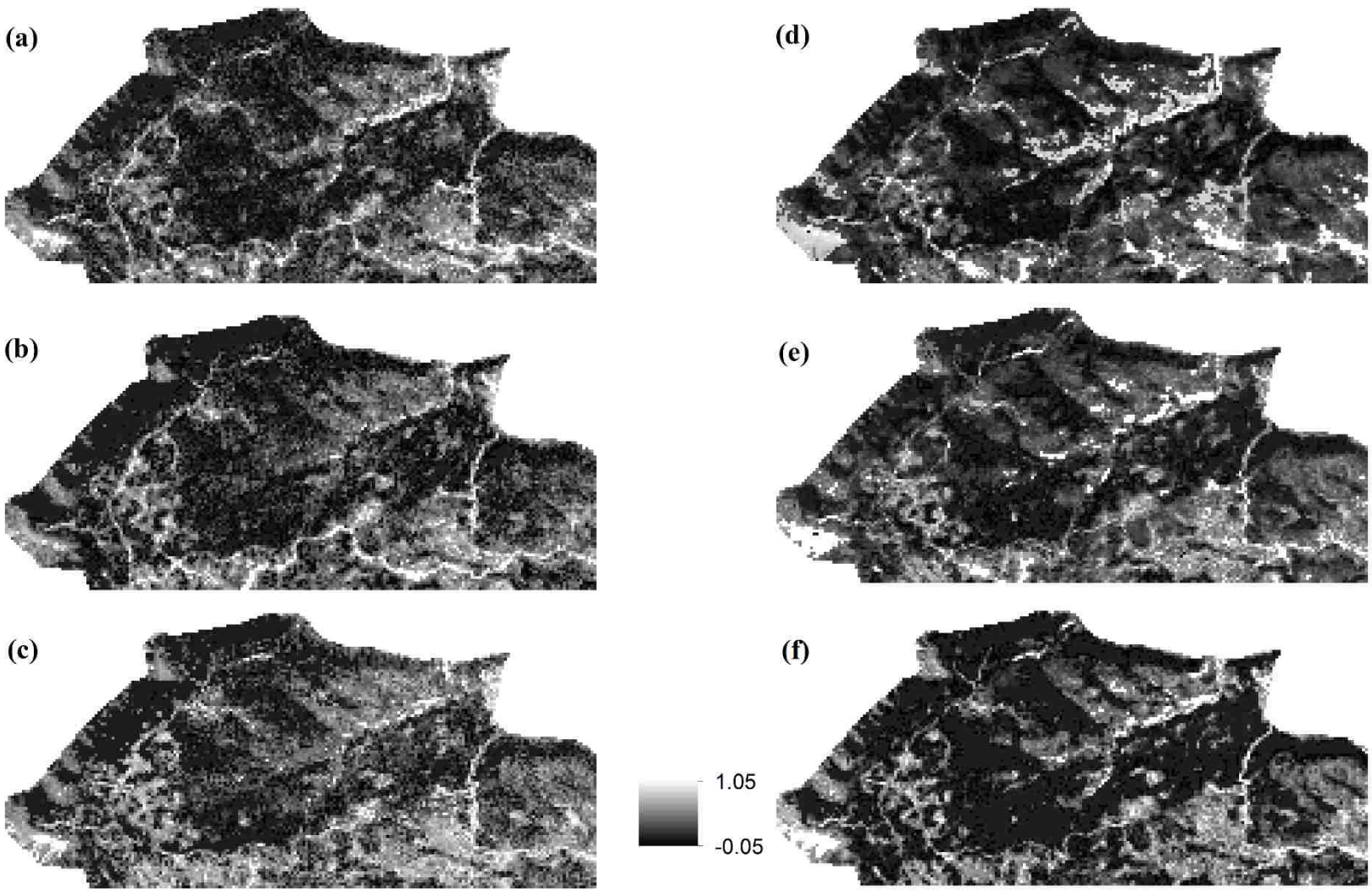

Figure 17. MESMA Soil proportions displayed in a stretched greyscale palette: a) 2009, b) 2010, c) 2011, d) 2013, e) 2014, f) 2015. Lighter tones represent higher Soil proportion, darker tones lower Soil proportion.

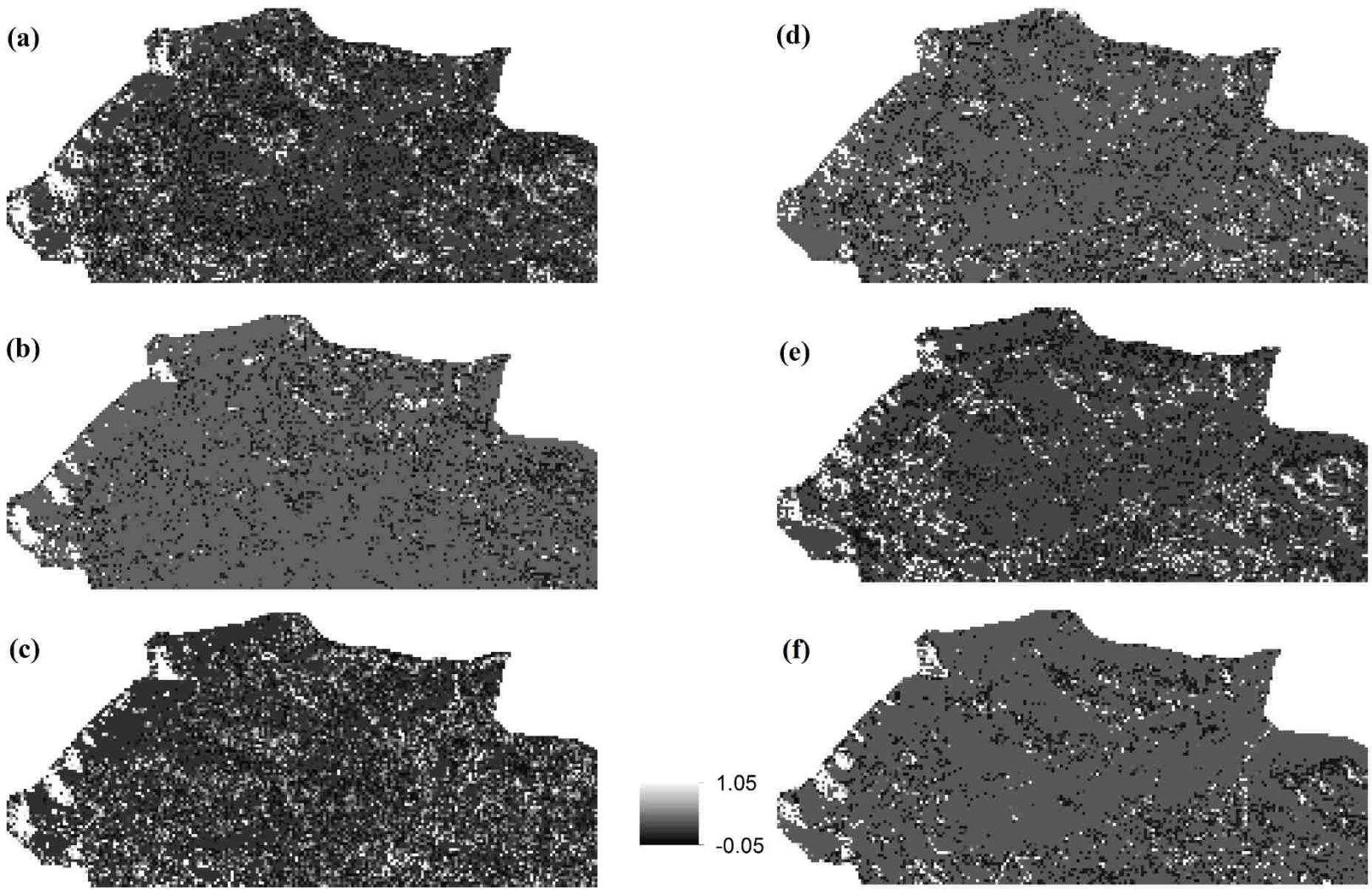

Figure 18. MESMA H proportions displayed in a stretched greyscale palette: a) 2009, b) 2010, c) 2011, d) 2013, e) 2014, f) 2015. Lighter tones represent higher H proportion, darker tones lower H proportion.

a)

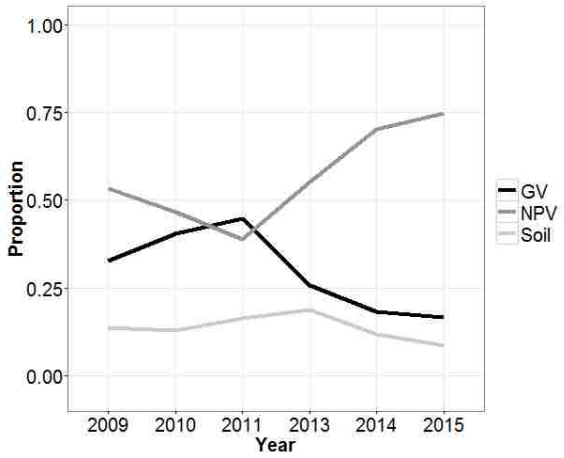

b)

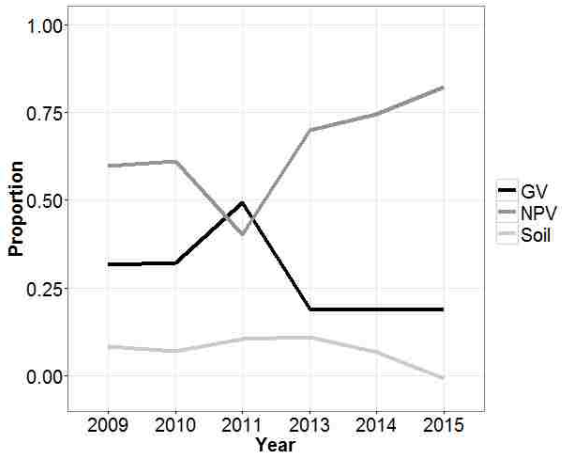

c)

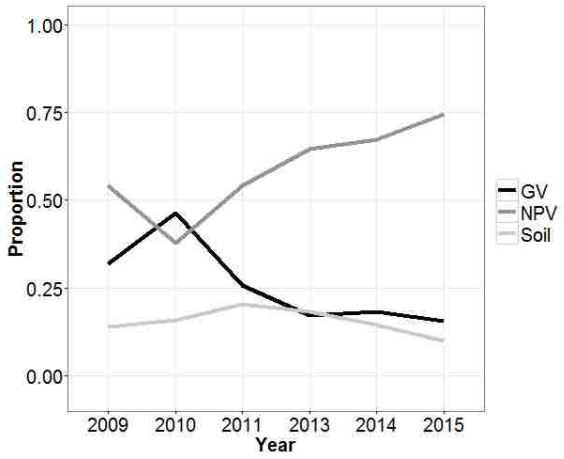

Figure 19. Change in fractional cover of soil, GV, and NPV across the study period at a) DCP, b) PJC, and c) PJG.

a)

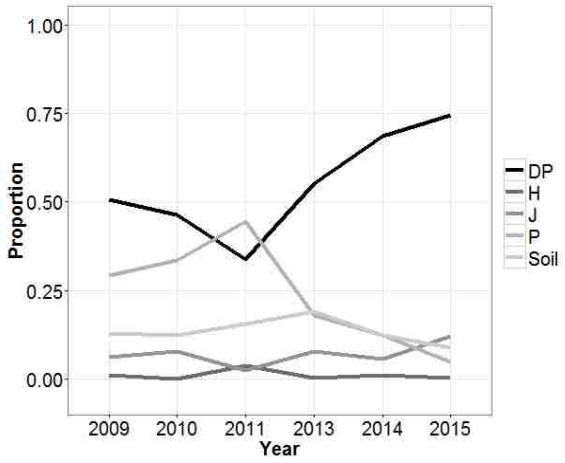

b)

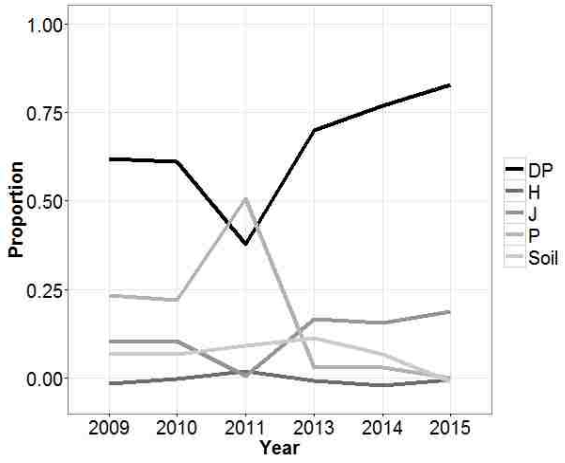

c)

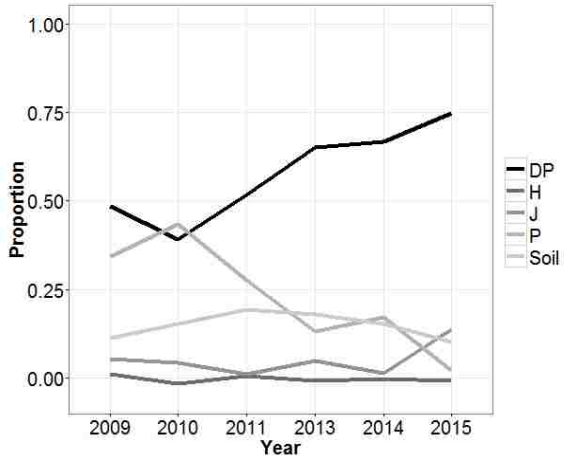

Figure 20. Change in fractional cover for all five classes (DP, H, J, P, and Soil) across the study period at a) DCP, b) PJC, and c) PJG.

Table 1. Selected Landsat image dates.

Year	Sensor	Month	Day of Month
2009	TM	May	10
2010	TM	April	27
2011	TM	April	30
2013	OLI	May	21
2014	OLI	April	22
2015	OLI	May	11

Table 2. Spectral sampling scheme.

Land Cover Type	Endmember	Sites
Piñon (P)	GV	20
Juniper (J)	GV	10
Dead Piñon (DP)	NPV	20
Herbaceous (H)	NPV	5
Bareground (Soil)	Soil	2

Table 3. Precipitation (mm) 2 weeks, 1 month (30 days), and 2 months (60 days) prior to Landsat imagery collection date.

Image Collection Date	**2 weeks**	**1 month**	**2 month**
May 10, 2009	0.7	11.5	13.9
April 27, 2010	26.2	26.2	73.3
April 30, 2011	0	0.7	3
May 21, 2013	3.2	4	9.1
April 23, 2014	16.3	16.3	28
May 11, 2015	21.3	26.5	50.5

Table 4. Root Mean Square Error, Mean Absolute Error, and R^2 values for the modeled and reference fractions from 2014 and 2015 accuracy assessment dates.

2014					
	Soil	GV	NPV	DP	H
RMSE	0.022	0.027	0.031	0.273	0.26
MAE	0.016	0.021	0.026	0.269	0.256
R^2	0.946	0.632	0.961	0.854	0.182
2015					
RMSE	0.016	0.028	0.035	0.373	0.348
MAE	0.012	0.025	0.032	0.365	0.338
R^2	0.863	0.735	0.966	0.881	0.244

Table 5. Change in fractional cover for GV, NPV, and soil across the study period for Deer Creek Plateau, PJ Girdle, and PJ Control site.

	2009	2010	2011	2013	2014	2015	Δ 2009 – 2015
DCP							
Soil	13.7	12.7	16.2	18.8	11.7	8.4	-5.3
GV	32.7	40.5	44.8	25.8	18.1	16.6	-16.1
NPV	53.4	46.7	38.8	55.2	70.1	74.8	21.4
PJG							
Soil	13.9	15.7	20.2	18.2	14.5	9.9	-4
GV	31.9	46.4	25.7	17.1	18.3	15.5	-16.4
NPV	54.1	37.7	54.1	64.7	67.2	74.5	20.4
PJC							
Soil	8.3	6.9	10.4	11	6.7	-1	-9.3
GV	31.7	32.1	49.4	19	18.8	18.7	-13
NPV	59.9	61	40.2	70	74.5	82.3	22.4

Table 6. Change in fractional cover for all land cover classes across the study period for the Deer Creek Plateau (DCP), PJ Control (PJC), and PJ Girdle (PJG).

	2009	2010	2011	2013	2014	2015	Δ 2009 – 2015
DCP							
Soil	12.9	12.4	15.5	19	12.2	8.7	-4.2
DP	50.7	46.4	33.7	55.2	68.7	74.5	23.8
H	1.1	0	3.8	0.2	1.1	0.1	-1
J	6	7.6	2.3	7.7	5.5	11.9	5.9
P	29.2	33.5	44.6	17.9	12.4	4.7	-24.5
PJC							
Soil	6.6	6.7	9.1	11.2	6.7	-1.1	-7.7
DP	61.9	61.1	37.8	70	76.9	82.9	21
H	-1.7	-0.3	1.8	-0.9	-2.2	-0.7	1
J	10	10.5	0.5	16.6	15.6	18.8	8.8
P	23.2	22	50.7	3	3	0	-23.2
PJG							
Soil	11.1	15.1	19.1	17.8	15.3	10.2	-0.9
DP	48.4	39.2	51.7	65.2	66.7	74.8	26.4
H	1	-1.8	0.5	-0.9	-0.3	-0.8	-1.8
J	5.3	4.2	1	4.9	1.4	13.7	8.4
P	34.2	43.3	27.6	13	17	2.2	-32

References

Adams, J. B., Smith, M. O., & Gillespie, A. R. (1993). Imaging spectroscopy: Interpretation based on spectral mixture analysis. In VM Pieters, & P. Englert (Eds.), Remote geochemical Analysis: Elementa l and Mineralogical Composition. New York: Cambridge Univ.Press.7, 145-166.

Adams, J.B., D.E. Sabol, V. Kapos, R.A. Filho, D.A. Roberts, M.O. Smith, and A.R. Gillespie, 1995. Classification of multispectral images based on fractions of endmembers: Application to land cover change in the Brazilian Amazon, Remote Sensing of Environment, 52:137–154.

Allen, C. D., Macalady, A. K., Chenchouni, H., Bachelet, D., & et. al. (2010). A global overview of drought and heat-induced tree mortality reveals emerging climate change risks for forests. *Forest Ecology and Management, 259*, 660–684.

Breshears, D. D., Cobb, N. S., Rich, P. M., Price, K. P., Allen, C. D., Balice, R. G., … Meyer, C. W. (2005). Regional vegetation die-off in response to global-change-type drought. *Proceedings of the National Academy of Sciences*, *102*(42), 15144–15148.

Breshears, D. D., Myers, O. B., Meyer, C. W., Fairley J, B., Zou, C. B., Allen, C. D., … Pockman, W. T. (2009). Tree die-off in response to global change-type drought: mortality insights from a decade of plant water potential measurements. *The Ecological Society of America*, *7*(4), 185–189. doi:10.1890/080016

Clifford, M.J., Cobb NS, Buenemann M. 2011. Long-term tree cover dynamics in a pinyon–juniper woodland: climate-change-type drought resets successional clock. *Ecosystems* 14: 949–962.

Clifford, M. J., Rocca, M. E., Delph, R., Ford, P. L., & Cobb, N. S. (2008). Drought Induced Tree Mortality and Ensuing bark Beetle outbreaks in Southwestern Pinyon-Juniper Woodlands. *USDA Forest Service Proceedings*, *51*, 39–51.

Cracknell, A. P., (1998) Review article Synergy in remote sensing-what's in a pixel?, International Journal of Remote Sensing, 19:11, 2025-2047, DOI: 10.1080/014311698214848

Dennison, P. E., & Roberts, D. A. (2003). Endmember selection for mapping chaparral species and fraction using Multiple Endmember Spectral Mixture Analysis. *Remote Sensing of Environment*, 41, 123–135.

Dennison, P. E., Halligan, K. Q., & Roberts, D. A. (2004). A comparison of error metrics and constraints for Multiple Endmember Spectral Mixture Analysis and Spectral Angle Mapper. *Remote Sensing of Environment*, 93, 359–367.

Drake, N. A., Mackin, S., & Settle, J. J. (1999). Mapping vegetation, soils, and geology in semiarid shrublands using spectral matching and mixture modeling of SWIR AVIRIS imagery. *Remote Sensing of Environment*, 68, 12–25.

Duncan, J., Stow, D., Franklin, J., & Hope, A. (1993). Assessing the relationship between spectral vegetation indices and shrub cover in the Jornada Basin, New Mexico. *International Journal of Remote Sensing*, 14, 3395– 3416.

Eitel, J. U. H., Long, D. S., Gessler, P. E., Hunt, E. R., & Brown, D. J. (2009). Sensitivity of ground-based remote sensing estimates of wheat chlorophyll content to variation in soil reflectance. *Soil Science Society of America Journal*, 73, 1715.

Franklin, J., Duncan, J., & Turner, D. L. (1993). Reflectance of vegetation and soil in Chihuahuan desert plant communities from ground radiometry using SPOT wavebands. *Remote Sensing of the Environment*, 46, 291– 304.

Franklin, J. (2002). Enhancing a regional vegetation map with predictive models of dominant plant species in chaparral. *Applied Vegetation Science* 5:135- 146.

Gaylord ML, Kolb TE, Pockman WT, Plaut JA, Yepez EA, Macalady AK, Pangle RE, McDowell NG. (2013). Drought predisposes pi~non–juniper woodlands to insect attacks and mortality. *New Phytologist* 98: 567–578.

Illera, P., Fernandez, A., & Delgado, J. A. (1996). Temporal evolution of the NDVI as an indicator of forest fire danger. International Journal of Remote Sensing, 17 (6), 1093 – 1105.

IPCC. 2014. Climate change 2014: impacts, adaptation, and vulnerability. Part A: global and sectoral aspects. Contribution of Working Group II to the Fifth Assessment Report of the Intergovernmental Panel on Climate Change. Cambridge University Press, Cambridge, UK.

Kremer, R.G., Running, S.W., 1993. Community type differentiation using NOAA/AVHRR data within a sagebrush-steppe ecosystem. Remote Sensing of Environment 46, 311–318.

Krofcheck, Dan J., (2014). Bridging structure and function in semi-arid ecosystems by integrating remote sensing and ground based measurements. (Doctoral Dissertation).

Krofcheck, Dan J., Eitel, J. U. H., Vierling, L. A., Schulthess, U., Hilton, T. M., Dettweiler-Robinson, E., Pendleton, R., Litvak, M. E. (2014). Detecting mortality induced structural and functional changes in a piñon-juniper woodland using Landsat and RapidEye time series. *Remote Sensing of Environment*, *151*, 102–113.

Li, X., Gao, Z., Bai, L., & Huang, Y. (2012). Potential of high resolution RapidEye data for sparse vegetation fraction mapping in arid regions. Geoscience and Remote Sensing Symposium (IGARSS). 2012 IEEE International. (pp. 420–423).

Limousin, J.-M., Bickford, C.P., Dickman, L.T., Pangle, R.E., Hudson, P.J., Boutz, A.L.,Gehres, N., Osuna, J.L., Pockman, W.T., McDowell, N.G., 2013. Regulation andacclimation of leaf gas exchange in a piñon -juniper woodland exposed to threedifferent precipitation regimes. Plant Cell Environ. 36, 1812–1825.

Lippitt,C. L., (2013). Remote-Sensing Based Characterization of Herbaceous Vegetation in California Shrublands. (Doctoral Dissertation).

Logan, J.A., J. Regniere, and J.A. Powell. 2003. Assessing the impacts of global warming on forest pest dynamics. *Frontiers in Ecology and the Environment* 1: 130-137.

McDowell, N.G., White, S., Pockman, W.T., 2008. Transpiration and stomatalconductance across a steep climate gradient in the southern Rocky Mountains.Ecohydrology 1, 193–204.

Winter climate change promotes an altered spring growing season in piñon pine-juniper woodlands (PDF Download Available). Available from: https://www.researchgate.net/publication/281650977_Winter_climate_change_promotes_an_altered_spring_growing_season_in_piñon _pine-juniper_woodlands [accessed Apr 13, 2016].

Miller, Richard F.; Tausch, Robin J.; McArthur, E. Durant; Johnson, Dustin D.; Sanderson, Stewart C. 2008. Age structure and expansion of piñon -juniper woodlands: a regional perspective in the Intermountain West. Res. Pap. RMRS-RP-69. Fort Collins, CO: U.S. Department of Agriculture, Forest Service, Rocky Mountain Research Station. 15 p.

Mueller, R. C., Scudder, C. M., Porter, M. E., Talbot Trotter III, R., Gehring, C. A., & Whitham, T. G. (2005). Differential tree mortality in response to severe drought: evidence for long-term vegetation shifts. *Journal of Ecology*. doi:10.1111/j.1365-2745.2005.01042.

Myint, S. W., & Okin, G. S. (2009). Modelling land-cover types using Multiple Endmember Spectral Mixture Analysis in a desert city. *International Journal of Remote Sensing*, 30, 2237–2257.

Okin, G. S., Roberts, D. A., Murray, B., and Okin, W. J. (2001). Practical limits on hyperspectral vegetation discrimination in arid and semiarid environments. *Remote Sensing of Environment* 77: 212–225.

"Pinyon-Juniper Distribution (AZ, CO, NM, NV, UT)." *PJ-WIN Pinyon Juniper Woodlands Information Network*. Northern Arizona University, 17 Dec. 2008. Web. 21 Aug. 2015. <http://perceval.bio.nau.edu/MPCER_OLD/pjwin/pjmaps.htm>.

Palmer, Wayne. (1965)., "Meteorological Drought". Research paper no.45, U.S. Department of Commerce Weather Bureau.

Padien, D. J., & Lajtha, K.. (1992). Plant Spatial Pattern and Nutrient Distribution in Pinyon-Juniper Woodlands Along an Elevational Gradient in Northern New Mexico. *International Journal of Plant Sciences*, *153*(3), 425–433.

Paltridge, G. W., & Mitchell, R. M. (1990). Atmospheric and viewing angle correction of vegetation indices and grassland fuel moisture content derived from NOAA/AVHRR. Remote Sensing of Environment, 31, 121 – 135.

Peters, A.J., Eve, M.D., (1995). Satellite monitoring of desert plant community response to moisture availability. Environmental Monitoring and Assessment 37, 273–287.

Petrie MD, Pockman WT, Pangle RE, Limousin JM, Plaut JA and McDowell NG. (2016). Winter climate change promotes altered spring growing season in Piñon -juniper woodlands. Agricultural and Forest Meteorology. 214–215 (2015), 357–368.

Plaut, J.A., Yepez, E.A., Hill, J., Pangle, R., Sperry, J.S., Pockman, W.T., Mcdowell, N.G.,2012. Hydraulic limits preceding mortality in a piñon -juniper woodland underexperimental drought. Plant Cell Environ. 35, 1601–1617.

Quintano, C., Fernández-Manso, A., & Roberts, D. A. (2013). Multiple Endmember Spectral Mixture Analysis (MESMA) to map burn severity levels from Landsat images in Mediterranean countries. *Remote Sensing of Environment, 136*, 76–88. http://doi.org/10.1016/j.rse.2013.04.017

Raffa, K. F., Aukema, B. H., Bentz, B. J., Carroll, A. L., Hicke, J. A., Turner, M. G., & Romme, W. H. (2008). Cross-scale Drivers of Natural Disturbances Prone to Anthropogenic Amplification: The Dynamics of Bark Beetle Eruptions. *BioScience*, *58*(6), 501–517. http://doi.org/10.1641/B580607

Rennenberg, H., Loreto, F., Polle, A., Brilli, F., Fares, S., Beniwal, R.S., Gessler, A., 2006. Physiological responses of forest trees to heat and drought. Plant Biology 8, 556–571.

Rich, P.M., Breshears, D.D., & White, A.B. (2008). Phenology of mixed woody–herbaceous ecosystems following extreme events: Net and differential responses. *Ecological Society of America*, 89, 342–352.

Roberts, D.A., Gardner, M., Church, R., Ustin, S., Scheer, G.,and Green, R.O. 1998. Mapping chaparral in the Santa Monica mountains using multiple endmember spectral mixture models. *Remote Sensing of Environment* 65: 267-279.

Roberts, D. A., Dennison, P. E., Gardner, M. E., Hetzel, Y., Ustin, S. L., and Lee, C. T. 2003.Evaluation of the potential of Hyperion for fire danger assessment by comparison to the airborne visible/infrared imaging spectrometer. IEEE Transactions on Geoscience and Remote Sensing 41: 1297–1310.

Roberts, D. A., Ustin, S. L., Ogunjemiyo, S., and Greenberg, J. 2004. Spectral and structural measures of Northwest forest vegetation at leaf to landscape scales, Ecosystems 7:545-562.

Romme, W. H., Allen, C. D., Bailey, john D., Baker, W. L., Bestelmeyer, B., Brown, P., … Weisberg, P. (2009). Historical and Modern Disturbance Regimes, Stand Structures, and Landscape Dynamics in Piñon-Juniper Vegetation of the Western U.S. *Rangeland Ecology Management*, *62*, 203–222.

ViewSpec Pro™ User Manual. (2008). Boulder, CO: Analytical Spectral Devices, Inc.

Shaw, J. D., Steed, B. E., & Larry, D. T. (2005). Forest Inventory and Analysis (FIA) Annual Inventory Answers the Question: What Is Happening to Pinyon-Juniper Woodlands? *Jornal of Forestry*, 280–285.

Smith, M. O., Ustin, S. L., Adams, J. B., & Gillespie, A. R. (1990). Vegetation in deserts: I. A regional measure of abundance from multispectral images. *Remote Sensing of Environment*, 31, 1– 26.

Strahler, A. H., Woodcock, C. E., and Smith, J. A. 1986. On the nature of models in remote sensing, Remote Sens. Environ.20:121-139.

Tucker, C. J. (1977). Asymptotic nature of grass canopy spectral reflectance. Applied Optics, 16 (5), 1151 – 1156.

Tucker C (1979) Red and photographic infrared linear combinations for monitoring vegetation. Remote sensing of Environment 8(2):127–150, URL http://www.sciencedirect.com/science/article/pii/0034425779900130

Turner, MG. (1989). Landscape ecology: the effect of pattern on process. *Annual Review of Ecology Evolution and Systematics* 20: 171–197.

Williams, A. P., Allen, C. D., Millar, C. I., Swetnam, T. W., Michaelson, J., Still, C. J., & Leavitt, S. W. (2010). Forest responses to increasing aridity and warmth in the southwestern United States. *Proceedings of the National Academy of Sciences*, *107*(50), 21289–21294.

Williams, A. P., Allen, C. D., & Macalady, A. K. (2013). Temperature as a potent driver of regional forest drought stress and tree mortality. *Nature Climate Change*, *3*. doi:10.1038/NCLIMATE1693

Woolley, J. (1971). Reflectance and transmittance of light by leaves. *Plant Physiology*, vol. 47 no. 5 656-662.

Xiao, J., & Moody, A. (2005). A comparison of methods for estimating fractional green vegetation cover. *Remote Sensing of Environment*, (98), 237–250.

Yang, J., Weisberg, P. J., & Bristow, N. A. (2012). Landsat remote sensing approaches for monitoring long-term tree cover dynamics in semi-arid woodlands: Comparison of vegetation indices and spectral mixture analysis. *Remote Sensing of Environment*, *119*, 62–71.

Zeppel M.J.B., Lewis J.D., Chaszar B., Smith R.A., Medlyn B.E., Huxman TE.., Tissue, D.T., 2012. Nocturnal stomatal conductance responses to rising [CO2], temperature and drought. *New Phytologist* 193.